Intra-annual tree-ring $\delta^{18}O$ and $\delta^{13}C$ reveal a trade-off between isotopic source and humidity in moist environments

Guobao Xu [1, 2, 3]*, Xiaohong Liu [4, 1], Jia Hu [2,5], Isabel Dorado-Liñán [6, 2], Mary Gagen [7], Paul Szejner[2,8], Tuo Chen[1,]*, Valerie Trouet [2,5]

1. State Key Laboratory of Cryospheric Sciences, Northwest Institute of Eco-Environment and Resources, Chinese Academy of Sciences, Lanzhou 730000, China

2. Laboratory of Tree-Ring Research, University of Arizona, Tucson, 85721, USA

3. National Field Science Observation and Research Station of Yulong Mountain Cryosphere and Sustainable Development, Chinese Academy of Sciences, Lanzhou 730000, China

4. School of Geography and Tourism, Shaanxi Normal University, Xi'an 710119, China

5. School of Natural Resources and the Environment, University of Arizona, Tucson, 85721, USA

6. Forest Genetics and Ecophysiology Research Group, Technical University of Madrid, Madrid, Spain

7. Department of Geography, Swansea University, Singleton Park, Swansea SA2 8PP, UK

8. Instituto de Geología, Universidad Nacional Autónoma de México, México City 04510, México

Running Title: Intra-annual tree-ring $\delta^{18}O$ and $\delta^{13}C$ indicators

*** Authors for correspondence:**

Guobao Xu

E-mail: xgb234@lzb.ac.cn; guobaoxu@arizona.edu

Tel.: +86 15101229611

1. State Key Laboratory of Cryospheric Sciences, Northwest Institute of Eco-Environment and Resources, Chinese Academy of Sciences, Lanzhou 730000, China

2. Laboratory of Tree-Ring Research, University of Arizona, Tucson, 85721, USA

Tuo Chen

E-mail: chentuo@lzb.ac.cn

Tel.: +86 9314967373

1. State Key Laboratory of Cryospheric Sciences, Northwest Institute of Eco-Environment and Resources, Chinese Academy of Sciences, Lanzhou 730000, China

Supporting information:

Methods S1: Climate at our study site.

Methods S2: Coherent variability of precipitation $\delta^{18}O$ from observation and IsoGSM model.

Methods S3: Tree-ring stable isotope forward process-based models simulation and parameterization.

Methods S4: Design of modeling experiment and comparison between observations and simulations.

Figure S1-S12.

Table S1-S2.

Abstract

Tree-ring intra-annual stable isotopes ($\delta^{13}C$ and $\delta^{18}O$) are powerful tools for revealing plant ecophysiological responses to climatic extremes. We analyzed interannual and fine-scale intra-annual variability of tree-ring $\delta^{13}C$ and $\delta^{18}O$ in *Pinus massoniana* from southeastern China to explore environmental drivers and potential trade-offs between the main physiological controls. We show that wet season relative humidity (May-October RH) drove interannual variability of $\delta^{18}O$ and intra-annual variability of tree-ring $\delta^{18}O$. Interannual variability of tree-ring $\delta^{13}C$ was mainly driven by February-May temperature and September-October RH, whereas intra-annual variability was controlled by May-October RH. Furthermore, intra-annual tree-ring $\delta^{18}O$ variability was larger during wet years compared to dry years, whereas $\delta^{13}C$ variability was lower during wet years compared to dry years. As a result of these differences in intra-annual variability amplitude, process-based models (we used the Roden model for $\delta^{18}O$ and the Farquhar model for $\delta^{13}C$) captured the intra-annual $\delta^{18}O$ profile better in wet years compared to dry years, whereas intra-annual $\delta^{13}C$ profile was better simulated in dry years compared to wet years. This result suggests a potential asymmetric bias in process-based models in capturing the interplay of the different mechanistic processes (i.e., isotopic source and leaf-level enrichment) operating in dry versus wet years. We therefore propose an intra-annual conceptual model considering a dynamic trade-off between the isotopic source and leaf-level enrichment in different

tree-ring parts to understand how climate and ecophysiological processes drive intra-annual tree-ring stable isotopic variability under humid climate conditions.

Keywords:

phenology, intra-annual variability, leaf-level enrichment, stable carbon and oxygen isotopes in tree rings, ecophysiology, subtropical China, process-based model

1. Introduction

The mechanisms through which plants respond to gradual climatic changes and climate extremes are critical for understanding the influence of anthropogenic climate change on vegetation (McDowell *et al.*, 2010, Sternberg, 2009). Tree-ring stable carbon ($\delta^{13}C$) and oxygen ($\delta^{18}O$) isotopes are useful tools to study such plant functional and ecophysiological responses to climate change trends and climatic extremes (Farquhar *et al.*, 1982, Timofeeva *et al.*, 2017, Gessler *et al.*, 2014, Scheidegger *et al.*, 2000).

The $\delta^{13}C$ records fixed in tree rings contain information about the historical balance between carbon gain and water loss (Farquhar *et al.*, 1982). Therefore, tree-ring $\delta^{13}C$ records are valuable to understand tree responses to increasing CO_2 concentrations, photosynthetic rates, stomatal conductance rates, and the long-term effects after extreme climate (Farquhar *et al.*, 1982, Castagneri *et al.*, 2018, Timofeeva *et al.*, 2017, Szejner *et al.*, 2020a).

The isotopic fractionation during processes of gas exchange and carbon assimilation determines a large portion of what is fixed in tree-ring $\delta^{13}C$ ratios. Both are controlled by physiological mechanisms driven by climate and site conditions (Farquhar *et al.*, 1982). Under unlimited diffusion of CO_2 (i.e., open stomata), the tree will discriminate more strongly to ^{13}C compared to ^{12}C because the Rubisco enzyme reacts faster with $^{12}CO_2$ than $^{13}CO_2$ (Farquhar *et al.*, 1982). In response to drought stress, however, trees reduce stomatal conductance, which limits CO_2 diffusion, reducing the intercellular CO_2 concentrations (C_i), leading to more relative incorporation of ^{13}C

during carbon fixation and thus higher tree-ring $\delta^{13}C$ values (Farquhar *et al.*, 1982, Castagneri *et al.*, 2018).

Tree-ring $\delta^{18}O$ can unveil ecohydrological variability and plant responses to climate conditions (Song *et al.*, 2014, Gessler *et al.*, 2014, Treydte *et al.*, 2014). The $\delta^{18}O$ fixed in tree rings is mainly determined by isotopic content of the source water $\delta^{18}O$ used by the tree and the degree of leaf water $\delta^{18}O$ enrichment, which is negatively related to relative humidity (RH), and positively to water vapor pressure deficit (VPD) (Roden *et al.*, 2000, Barbour *et al.*, 2004, Kahmen *et al.*, 2011, Treydte *et al.*, 2014). When the soil evaporative enrichment is weak and no additional water source inputs (i.e., groundwater or snowmelt) exist, the source water $\delta^{18}O$ used by the shallow-rooted tree species is likely very similar to precipitation $\delta^{18}O$ (Treydte *et al.*, 2014, Kahmen *et al.*, 2011, Allen *et al.*, 2019). Precipitation $\delta^{18}O$, in turn, is affected by temperature, precipitation amount, and original water source (Dansgaard, 1964), which may imprint a climatic signal in tree-ring $\delta^{18}O$ (Treydte *et al.*, 2014). Leaf water $\delta^{18}O$ fractionation can be further modified by the Péclet effect (Farquhar & Lloyd, 1993, Barbour *et al.*, 2004), which is still difficult to measure and can be a species-specific parameter (Song *et al.*, 2014, Gessler *et al.*, 2013, Cernusak *et al.*, 2016). In addition, P_{ex}, the proportion of sugars that exchange with xylem water during cellulose synthesis, affects the $\delta^{18}O$ value fixed in tree rings. Moreover, some evidence suggests that P_{ex} can increase with drought (Cheesman and Cernusak, 2017, Szejner et al., 2020b).

Interannual tree-ring $\delta^{13}C$ and $\delta^{18}O$ measurements have been used to explore plant

responses to climate variability (Kahmen *et al.*, 2011, Roden & Siegwolf, 2012), forest dynamics (e.g., forest thinning) (Sohn *et al.*, 2012), and environmental changes (e.g., Xu *et al.*, 2020a, McCarroll & Loader, 2004). However, such annual-level isotopic measurements integrate information over the entire growing season and therefore limit our understanding on the intra-annual or seasonal ecophysiological responses (Helle & Schleser, 2004, Szejner et al. 2021, Belmecheri et al 2022). Fine-resolution (i.e., intra-annual, seasonal, and subseasonal) measurements of stable isotopes in tree-ring may provide critical information about seasonal changes of source water uptake by trees (Treydte *et al.*, 2014), as well as about interactions with prevailing climatic conditions, soil moisture variability, and adaptive physiological responses to drought (Schollaen *et al.*, 2014, Rinne *et al.*, 2015, Schubert & Jahren, 2015, Castagneri *et al.*, 2018). For example, the seasonal variability of earlywood (EW) and latewood (LW) tree-ring $\delta^{13}C$ and $\delta^{18}O$ has provided valuable information about legacy effects within and between subsequent growing seasons (Szejner *et al.*, 2018, Castagneri *et al.*, 2018). In other cases, intra-annual tree-ring $\delta^{18}O$ revealed the seasonal cyclic signal of source water $\delta^{18}O$ and the influence of drought on leaf-water enrichment in different portions (i.e., EW and LW) (Belmecheri *et al.*, 2018, Xu *et al.*, 2020a), as well as the P_{ex} and the peclet effect (Cernusak *et al.*, 2016, Szejner *et al.*, 2020b). In tropical and sub-tropical regions, intra-annual tree-ring $\delta^{13}C$ and/or $\delta^{18}O$ analyses have been used to explore El Niño Southern Oscillation signals (Evans & Schrag, 2004, Anchukaitis & Evans, 2010, Zhu *et al.*, 2012a, Xu *et al.*, 2016, van der Sleen et al., 2017), precipitation variability

(Schubert & Jahren 2011, Schubert & Timmermann, 2017), and seasonal climatic divergence (Xu *et al.*, 2020a).

Intra-annual measurements of tree-ring $\delta^{13}C$ and $\delta^{18}O$ can therefore broaden our understanding of the mechanisms orchestrating stable isotope signal transfers from the environment to the leaves and to tree rings, as well as tree responses to climate extremes (Gessler *et al.*, 2014, Schollaen *et al.*, 2014, Rinne *et al.*, 2015). However, due to intrinsic methodological constraints (such as barriers of cost, difficulties in isolating intra-annual cellulose samples, and labor- and time-consuming procedures) (Schollaen *et al.*, 2014, Castagneri *et al.*, 2018, Belmecheri *et al*., 2022), most intra-annual tree-ring $\delta^{13}C$ and $\delta^{18}O$ investigations have been limited to only a few years of analyses, limiting inference of the intra-annual profile and the study of interactions between climate variability and isotopic composition in tree rings at multiple time-scales (i.e. subseasonal to decadal). As a result, some questions remain unexplored, such as what additional information about climate extremes do we gain from understanding the intra-annual variability in tree-ring stable isotopes compared to annual measurements of isotopes? Do existing process-based models capture the intra-annual tree-ring stable isotope variability and reproduce the main mechanisms during extreme climatic events?

To address these questions, we used two 115-year-long (1900-2014 CE) intra-annually resolved tree-ring $\delta^{13}C$ and $\delta^{18}O$ chronologies of *Pinus massoniana* (Chinese red pine) from southeastern China. Parts of these chronologies were previously used to detect the climatic signals in intra-annual $\delta^{18}O$ extremes (Xu *et al.*, 2020a). Here, we

aim to determine the climatic drivers, as well as the mechanisms governing interannual variability, as well as intra-annual profiles of tree-ring $\delta^{13}C$ and $\delta^{18}O$. Our main hypotheses are: 1) interannual variability and intra-annual profiles of tree-ring $\delta^{13}C$ and $\delta^{18}O$ have different climatic drivers, 2) tree-ring $\delta^{13}C$ and $\delta^{18}O$ intra-annual profiles differ between dry and wet years, 3) these differences reflect the interplay between dynamic mechanisms governing intra-annual profiles in tree-ring $\delta^{13}C$ and $\delta^{18}O$, such as changes in the strength of stomatal control or leaf-water enrichment, and 4) process-based models can reliably reproduce the observed intra-annual profiles in tree-ring $\delta^{13}C$ and $\delta^{18}O$, particularly in dry years when climatic constraints are stronger than in wet years.

By testing these hypotheses, we propose an intra-annual conceptual model in which the main mechanistic process varies for each section of the tree ring (i.e., early-EW and late-LW parts) in order to explain the mechanism governing intra-annul tree-ring $\delta^{13}C$ and $\delta^{18}O$ responses in dry and wet years. This study will provide a benchmark for how tree-ring $\delta^{13}C$ and $\delta^{18}O$ process-based models can reproduce intra-annual tree-ring $\delta^{13}C$ and $\delta^{18}O$ profiles during extreme climate events.

2. Data and methods

2.1 Sampling site and climate data

The sampling site is located near Zhurong Peak (112.70°E, 27.27°N, 603 m a.s.l.) in the Hengshang Mountains in southeastern China (Figure 1), with a slope of about 20

degrees and with limited tree-to-tree canopy competition. The soil type is gleysols with a depth of 50 cm. As an East Asian monsoonal site (Ding & Chan, 2005), the study site is characterized by a wet season that lasts from March to October, which includes wet spring (March-May) and a relatively dry late-summer (July-August) and autumn (September-November) conditions (Figure 1; supplementary S1). Micro-coring studies on *Pinus massoniana* near our site revealed a xylem growth period spanning from late-February/March to December, with semi-dormancy in December (Huang *et al.*, 2018, Huang *et al.*, 2020). We therefore define the growing season as February to December.

We obtained monthly meteorological data from the Nanyue station (112.75°E, 27.25°N, 1130 m a.s.l.; 1953-2014) from the China Meteorological data service center (http://data.cma.cn/en). The climate variables we used in our analysis include mean (TEM), maximum (TMAX), and minimum (TMIN) temperature, monthly precipitation (PRE), relative humidity (RH), evaporation (EVP), and sunshine duration hours (SSD). We estimated the diurnal temperature range (DTR) as the difference between TMAX and TMIN.

We further estimated monthly vapor pressure deficit (VPD) based on RH and TEM (Bolton, 1980) as follows:

$$\mathrm{VPD} = 6.11 \times \exp^{\left(\frac{17.67 \times T}{243.5+T} \times \frac{1-RH}{100}\right)}, \quad (1)$$

where the T is the mean monthly air temperature (°C) and *RH* (%) is the mean monthly relative humidity.

197 **2.2 Crossdating and stable isotopes analysis**

198 We collected tree-ring cores (2 cores per tree) from 36 *Pinus massoniana* trees
199 (70-210 years) with a 12-mm increment borer (Haglof, Sweden). We measured tree-
200 ring widths (TRW) using a LINTAB 6.0 platform (Rinntech, Heidelberg, Germany) and
201 crossdated the samples using standard dendrochronological methods (Cook &
202 Kairiukstis, 1990). We then selected cores from four mature (110 to 180 years in age)
203 trees (one core per tree except for tree D, from which we used two cores in stable isotope
204 analysis: core B for 1950-2006 and core A for six additional years: 2007-2010, 2013,
205 and 2014; Figure S2) that displayed similar TRW variability (Figure S1) to establish
206 sequential intra-annual isotope chronologies for the period 1900-2014. In addition to
207 total TRW, we also visually distinguished EW and LW boundaries for these cores and
208 measured EW and LW width separately.

209 Each tree ring of the five selected cores was split into multiple sequential 200-μm
210 thin sections using a rotary microtome (HM340, Themero Scientific, Waltham MA,
211 USA). We used sections of 100 or 150 μm for some of the narrowest tree rings to obtain
212 sufficient sub-annual samples (Xu *et al.*, 2020a). We obtained 4 to 42 thin sections per
213 tree ring and annotated for each thin section whether it was derived from the EW or LW.
214 In total, we obtained 4611 thin-section samples (Figure S2). We then extracted α-
215 cellulose from each sample using the Teflon Filter-57 bag method (Leavitt & Danzer,
216 1993) according to the procedures described by (Loader *et al.*, 1997). We homogenized

the α-cellulose using an ultrasound machine (JY92-2D, Scents Industry, Ningbo, China) and then freeze-dried at -40°C for stable isotope measurement.

For $\delta^{13}C$ and $\delta^{18}O$ measurements, we packed 160-190 μg of α-cellulose into silver capsules. We simultaneously measured $\delta^{13}C$ and $\delta^{18}O$ at a temperature of 1400°C for furnace and 65°C for gas chromatograph using a high-temperature-conversion elemental analyzer (TC/EA; Thermo Electron Corporation, Bremen, Germany) coupled to a MAT-253 mass spectrometer (Thermo Electron Corporation) at the State Key Laboratory of Cryospheric Sciences, Chinese Academy Sciences, Lanzhou, China. This method of simultaneous measurement of $\delta^{13}C$ and $\delta^{18}O$ has been used in many studies (Xu *et al.*, 2018, Loader *et al.*, 2014, Andreu-Hayles *et al.*, 2018, Evans *et al.*, 2016). More details such as reference materials (Sigma-Aldrich α-cellulose, IAEA-CH3 standard, and benzoic acid IAEA 601), measurement conditions (1.2 bar for He carrier gas), and calibration method (two-point calibration) can be found in Xu et al. (2018). For samples for which the standard deviation was higher than 0.30‰ for $\delta^{18}O$ and 0.15‰ for $\delta^{13}C$, we measured each sample twice or three times. The final uncertainties of the repeated sample measurements were approximately 0.2‰ for $\delta^{18}O$ and 0.1‰ for $\delta^{13}C$.

2.3 Intra-annual tree-ring $\delta^{13}C$ and $\delta^{18}O$ assignment

Forty-five percent of the $\delta^{13}C$ and $\delta^{18}O$ measurements across all cores and years were EW measurements and 55% were LW measurements. Because different tree rings were sectioned into a different number of samples, we used the tracheidogram method

(Vaganov, 1990) to develop intra-annual time series using the R package "tgram" (DeSoto *et al.*, 2011) (Figure 2a). Approximately 80% of the rings were sectioned into more than 10 samples and we therefore used a scale of 10 values (EW1 to EW5 and LW1 to LW5). We divided EW and LW measurements into an even number (5) of thin sections, to allow for comparison between years. This decision was further based on a study of *pinus massinuana* at Shimentai (24°23′53″N, 113°11′56″E, 261m a.s.l.), a site near our sampling site, which showed that the number of wall-thickening cells and the number of xylem cells varied little throughout the growing season (Huang *et al.*, 2018).

We evaluated coherency in the variability of intra-annual tree-ring $\delta^{13}C$ and $\delta^{18}O$ samples series between trees using a mean correlation between all pairs of series (Rbar; using 35-year lags over 15 years running windows) for the maximum period of overlap using the "dplR" package (Bunn, 2010). We then averaged tree-ring $\delta^{13}C$ or $\delta^{18}O$ values for the same section (EW1 to LW5) of the same year for the four trees to obtain a site-level chronology for each of the 10 (EW1 to LW5) sections per year.

2.4 Climate response and intra-annul tree-ring $\delta^{13}C$ and $\delta^{18}O$ profiles in dry and wet years

To detect climate signals in tree-ring $\delta^{13}C$, we corrected raw intra-annual tree-ring $\delta^{13}C$ series ($\delta^{13}C_{raw}$) taking into account the decreases in atmospheric $\delta^{13}C$ ($\delta^{13}C_{atm}$) since 1850, also called the "Suess effect", by adding the difference of $\delta^{13}C_{atm}$ into the $\delta^{13}C_{raw}$ (McCarroll & Loader, 2004). We corrected the intra-annual tree-ring $\delta^{13}C$ data using the annual $\delta^{13}C_{atm}$ data due to lack of long-term intra-seasonal $\delta^{13}C_{atm}$

257 measurements. Annual $\delta^{13}C_{atm}$ values for the correction were obtained from Belmecheri
258 and Lavergne (2020) from 1900 to 2014. We refer to the corrected series as $\delta^{13}C_{cor}$.

259 We evaluated the climate response of tree-ring $\delta^{13}C_{cor}$ and $\delta^{18}O$ by correlating each
260 section (EW1 to LW5) chronology with various climate variables over the common
261 period (1953-2014). We conducted climate response analyses for the time window
262 spanning from February of the year previous to the growth year to December of the
263 growth year in the R package "treeclim" (Zang & Biondi, 2015).

264 We compared mean values and intra-annual profiles of tree-ring $\delta^{13}C_{cor}$ and $\delta^{18}O$
265 during dry, wet, hot, and cold years. We defined dry and wet years over the observation
266 period (1953-2014) as the 10th (RH = 84.2%) and 90th (RH = 89.5%) percentile for the
267 growing season RH, respectively, and defined cold and hot years as the 10th (TEM =
268 14.3℃) and 90^{th} (TEM = 15.7℃) percentile for the growing season temperature. We
269 define dry and wet years based on the growing season RH because it combines the
270 effects of both temperature and moisture conditions and thus generally shows strong
271 climatic signals in tree-ring isotopes (Xu et al., 2020). Furthermore, we found that dry
272 and wet years as defined based on the growing season RH are same as those years
273 defined based on the growing season VPD (results not shown). Additionally, we tested
274 differences in mean values of tree-ring stable isotopes between the two types of years
275 (i.e., dry versus wet and hot versus cold) using a Wilcoxon test and compared the intra-
276 annual position of the minimum $\delta^{13}C_{cor}$ and $\delta^{18}O$ values between these two types of
277 years.

2.5 Tree-ring $\delta^{13}C$ and $\delta^{18}O$ model simulations and sensitivity

We simulated tree-ring $\delta^{13}C$ variability using the Farquhar model (Farquhar et al., 1982; Supplementary Methods S3). To maintain the seasonal patterns of $\delta^{13}C_{atm}$, we used monthly $\delta^{13}C_{atm}$ values from the Mauna Loa station (155.6°E, 19.5°N, 3397 m a.s.l.; 1959-1990) and the Waliguan station (100.90°E, 36.28°N, 3810 m a.s.l.; 1991-2014) (https://gml.noaa.gov/aftp/data/trace_gases/co2c13/flask/surface/) as input in the Farquhar model. We assumed that C_i/C_a is linearly related to leaf-air vapor pressure deficit (VPD) (Zhang & Nobel, 1996) (more details in Supplementary Methods S3).

Tree-ring $\delta^{18}O$ variability in α-cellulose was modeled using the Roden model (Roden *et al.*, 2000) (Methods S3). For the Roden model, our simulation experiment was limited to the period of overlap between the climate data, precipitation $\delta^{18}O$, and water vapor $\delta^{18}O$ data (1953-2010). We used growing-season $\delta^{18}O$ values of precipitation and water vapor at the nearest grid point (112.5°E, 27.62°E) from the IsoGSM model (Yoshimura, 2015) as input data because the precipitation $\delta^{18}O$ from the IsoGSM model showed coherent intra- and inter-annual variability with the observed precipitation $\delta^{18}O$ at the Changsha station (113.1°E, 28.2°E) from the Global Network of Isotopes in Precipitation database (Methods S2; Figure S3). More details about the two process-based models and their parameterizations can be found in the supplement (Table S2; Methods S3 and S4).

We tested to what extent the model output is sensitive to a particular parameter

(i.e., temperature and RH, Table 1) by changing each parameter and setting the other parameters as constants (i.e., mean value over the whole simulation period) and defined the simulation run as the contribution of the single parameter (Lavergne *et al.*, 2017). These model simulations can help to explore the main processes (i.e., leaf-water enrichment) that drive variability of tree-ring $\delta^{13}C$ and $\delta^{18}O$ in dry years and wet years. We compared the variability of tree-ring $\delta^{13}C$ and $\delta^{18}O$ between observed and modeled results at annual and intra-annual (i.e., monthly) time scales (Methods S4). To make the intra-annual comparison possible, we assumed that the ten sections were evenly distributed from February to November and from March to December based on the limited variability in intra-growing season radial growth in *pinus massinuana* (Huang *et al.*, 2018). Our selection of seasonality takes into account that the growing season and timing of xylem activities (xylogenesis) differ between years and between trees (Rossi et al., 2012). Thus, we conducted a seasonality sensitivity test to establish whether the growing season selection affected the intra-annual tree-ring $\delta^{13}C$ and $\delta^{18}O$ profiles (Method S3). The model results- obtained from the model being either fully parameterized with real-time climatic data (hereafter, full model) or partially parameterized by varying a single parameter- were compared against tree-ring stable isotopes measurements during dry and wet years to explore which processes or parameters exerted the largest influence on the intra-annual $\delta^{13}C$ and $\delta^{18}O$ profiles.

3. Results

3.1 Intra- and inter-annual variability of tree-ring $\delta^{18}O$ and $\delta^{13}C$

The Rbar values for the annual mean, EW, and LW $\delta^{18}O$ chronologies of the four trees ranged from 0.43 to 0.69 (Table S1). This result confirms that a limited number of trees can contain a strong enough common signal at intra-annual scales to develop site-level tree-ring $\delta^{18}O$ chronologies, which is supported by annual tree-ring $\delta^{18}O$ studies (Liñán et al., 2011). $\delta^{18}O$ series based on each of the 10 sections (EW1 to LW5) showed similarly strong interannual variability (Figure 2a, b; r = 0.2 to 0.87, $p < 0.05$, Figure S4a).

The intra-annual tree-level and site-level $\delta^{18}O$ profiles showed a coherent "V" pattern over the growing season and tracked precipitation $\delta^{18}O$ variability: $\delta^{18}O$ decreased from start to end of the EW (EW1 to EW5; early to mid-growing season) and increased from start to end of the LW (LW1 to LW5; mid- to late growing season; Figures 2c, 2d, S5). The most depleted (minimum) tree-ring $\delta^{18}O$ value thus occurred at the center of the tree ring (Figure 2c).

The Rbar values for the annual mean, EW, and LW $\delta^{13}C_{raw}$ chronologies of the four trees were low and ranged from -0.02 to 0.63, with a mean value of 0.42 for EW and 0.49 for LW (Table S1). Despite lower Rbar values in $\delta^{13}C_{raw}$ compared to $\delta^{18}O$, there was still evidence of a common signal in $\delta^{13}C_{raw}$ from different trees and tree-ring $\delta^{13}C_{cor}$ series showed similarly strong interannual variability (Figure 3a, b; r = 0.53

337 to 0.87, $p < 0.05$, Figure S4b).

338 The intra-annual $\delta^{13}C$ profile of individual trees and their average showed an
339 asymmetric inverse-V pattern (Figures 3c, S6): a gradual increase from the start of the
340 growing season (EW1) to a maximum in the second half of the LW (LW3 and LW4)
341 and a progressive decrease towards the end of the growing season (LW5) (Figures 3,
342 S6). The intra-annual $\delta^{13}C_{cor}$ profile showed a similar intra-annual pattern to that of
343 VPD (Figure 1c) and growing-season $\delta^{13}C_{atm}$ from the Waliguan station, although the
344 tree-ring $\delta^{13}C_{cor}$ peak is time-lagged (Figure 3d). Specifically, $\delta^{13}C_{atm}$ and VPD peaks
345 occurred in July-August, corresponding to a transition period from EW to LW (Huang
346 et al., 2018), when the tree-ring $\delta^{13}C_{cor}$ was not yet at its maximum.

347 **3.2 Climatic signals in interannual seasonal $\delta^{18}O$ and $\delta^{13}C$ variability**

348 Interannual variability in EW (EW1 to EW5) tree-ring $\delta^{18}O$ series were primarily
349 affected by moisture conditions of the previous year (Figure 4a-e). EW $\delta^{18}O$ series were
350 significantly ($p < 0.05$) positively correlated with VPD ($r = 0.49$ to 0.63), SSD ($r = 0.45$
351 to 0.60), and EVP ($r = 0.4$ to 0.6) and negatively correlated with RH ($r = -0.47$ to -0.64)
352 and PRE ($r = -0.28$ to -0.36) in October and November of the previous year.

353 Moisture conditions during the growing season were also the main climatic drivers
354 in LW (LW1-LW5) $\delta^{18}O$ variability, but their influences were strongest in the current
355 year (Figure 4f-j). Like EW $\delta^{18}O$ series, LW $\delta^{18}O$ series were significantly ($p < 0.05$)
356 positively correlated with VPD ($r = 0.28$ to 0.64), SSD ($r = 0.26$ to 0.54), and EVP ($r =$

0.30 to 0.56) and negatively correlated with RH (r = −0.27 to −0.66) and PRE (r = −0.25 to −0.44) in August to October of the current year. We found no significant temperature signal in LW $\delta^{18}O$. Both EW and LW $\delta^{18}O$ interannual variability showed weak correlations (r = 0.1 to 0.30) with monthly precipitation $\delta^{18}O$ (not shown).

Interannual variability in EW and LW $\delta^{13}C_{cor}$ was influenced by both temperature and moisture conditions (Figure 5). Both EW and LW $\delta^{13}C_{cor}$ were significantly (p < 0.05) positively correlated with TMIN (r = 0.25 to 0.47), TMAX (r = 0.25 to 0.36), and TMEAN (r = 0.25 to 0.42) in October and November from the previous year, and February to May and October to November of the current year (Figure 5). Both EW and LW $\delta^{13}C_{cor}$ showed weak correlations ($|r|$ = 0.25) with climate variables of February to May of the previous year. EW $\delta^{13}C_{cor}$ series were significantly (p < 0.05) correlated with PRE (r_{min} = −0.43) in October of the previous year and with VPD (r_{max} = 0.50) and RH (r_{min} = −0.45) in April of the current year (Figure 5a-e). LW $\delta^{13}C_{cor}$ series were significantly negatively correlated with RH (r = −0.25 to −0.55) and positively correlated with VPD (r = 0.24 to 0.52) in September and October of the current year (Figure 5f-j).

3.3 Climatic extremes affect intra-annual profile in observations and simulations

Tree-ring $\delta^{18}O$ values were significantly lower (0.5‰ to 2.3‰; p < 0.01) and the slopes of intra-annual variability were steeper during wet years compared to dry years (Figure 6a, 6b). The largest differences between wet and dry years occurred in the

central parts (EW5-LW2) of the ring, when tree-ring $\delta^{18}O$ was at an annual minimum (Figures 6b, 2c). PRE, RH, and VPD significantly ($p < 0.05$) differed between wet years and dry years (Figure S7, supplementary S1). However, we found no significant differences in monthly precipitation $\delta^{18}O$ profiles and mean values between wet and dry years (Figures 6c, S8). The tree-ring $\delta^{18}O$ minima showed a normal distribution (Kurtosis = −0.17 and Skewness = -0.32) in wet years but a platykurtic normal distribution (Kurtosis = −1.0 and Skewness = -0.12) in dry years (Figure 6d). $\delta^{18}O$ minima occurred in the central part of the tree-ring more often in wet years compared to dry years (Figure 6d). Temperature extremes affected intra-annual tree-ring $\delta^{18}O$ profiles less than RH and tree-ring $\delta^{18}O$ values were not significantly different between hot years and cold years (Figure S9a). Tree-ring $\delta^{18}O$ was only 0.4‰ to 0.7‰ higher in the three middle sections (EW5-LW2) during hot years compared to cold years (Figure S9b). Minimum tree-ring $\delta^{18}O$ values mostly occurred earlier in hot years compared to cold years (Figure S9d).

Tree-ring $\delta^{13}C_{cor}$ values throughout the ring were significantly lower (0.2‰ to 0.9‰, $p < 0.05$) in wet years compared to dry years (Figure 7). Moreover, the intra-annual $\delta^{13}C_{cor}$ profile was more consistent among wet years than among dry years, with less pronounced increasing trends towards the LW. Differences between wet and dry years were particularly large in the late-LW (LW2-LW5) $\delta^{13}C_{cor}$, with the largest difference in LW5 (-0.9‰; Figure 7b). The $\delta^{13}C_{cor}$ minimum occurred at the start of the ring (EW1-2) in dry years, but at the end of the ring (LW4-5) in wet years (Figure 7c).

398 $\delta^{13}C_{cor}$ values were consistently 0.5 to 0.8‰ higher in hot years compared to cold years,
399 but there was no difference in intra-annual profile patterns (Figure S9). As a result, in
400 the following process-based analyses, we focus on the inter-annual variability and intra-
401 annual profile of tree-ring $\delta^{13}C$ and $\delta^{18}O$ in wet and dry years, rather than hot and cold
402 years.

403 Intra-annual and inter-annual tree-ring $\delta^{18}O$ variability simulated by the Roden
404 model showed similar variability to that in our measurements ($r_{intra\text{-}annual} = 0.42$ and $r_{inter\text{-}}$
405 $_{annual} = 0.53$, $p < 0.001$, 1953-2010; Figure 8a, 8b). When selecting a March to December
406 growing season (rather than February to November), the correlation coefficients were
407 similar (Figure S11). The $\delta^{18}O$ simulation driven only by leaf-water enrichment
408 processes followed the observed intra-annual tree-ring $\delta^{18}O$ profile, but simulations
409 driven by source water only or by the full model diverged from the observed profile of
410 tree-ring $\delta^{18}O$ (Figure 8b). In dry years, the source water and full model simulations
411 showed distinct V-shape intra-annual $\delta^{18}O$ profiles, whereas observations showed more
412 constant values (Figure 8c). The enrichment simulation was able to reproduce the
413 observed intra-annual profile ($r = 0.58$, $p < 0.01$; Figure 8c, 8e). In wet years, both
414 model simulations and observations showed comparable V-shape patterns (Figure 8d).
415 The source water ($r = 0.61$, $p < 0.01$) and full model ($r = 0.64$, $p < 0.01$) simulations
416 were strongly correlated with the observed tree-ring $\delta^{18}O$ profile in wet years (Figure
417 8f).

418 When simulating tree-ring $\delta^{13}C$ variability, the full Farquhar-model (considering

419 temperature, RH, and $\delta^{13}C_{atm}$; Table 1) shows good skill ($r > 0.5$) (Figure 9a). For the
420 single parameter simulation, $\delta^{13}C_{atm}$ leads to a long-term decreasing trend in tree-ring
421 $\delta^{13}C$, whereas climate drives the year-to-year variability (Figure 9a). $\delta^{13}C$ simulations
422 based on temperature alone showed reduced inter-annual fluctuation compared to
423 simulations based on RH or climate (temperature and RH). After removing the long-
424 term linear trend from the intra-annual simulated and measured $\delta^{13}C$ time series,
425 measurements were more similar to simulations when accounting for climate,
426 temperature, and RH compared to simulations -accounting only for $\delta^{13}C_{atm}$ (Figure
427 S11a). The intra-annual $\delta^{13}C$ profile was consistent between observations and model
428 simulations based on $\delta^{13}C_{atm}$, climate, and the full model (Figures 9b, S11b), but
429 measured and simulated values largely diverged at the start and end of the rings. The
430 $\delta^{13}C$ profiles were similar but with nearly constant offsets (0.2~0.3‰) between
431 observations and model simulations based on $\delta^{13}C_{atm}$ in dry ($r = 0.5$; $p < 0.01$) and wet
432 years ($r = 0.74$; $p < 0.01$) (Figures 9c-f): in dry years, observed $\delta^{13}C$ was higher (Figures
433 9c, S11c), whereas in wet years $\delta^{13}C_{atm}$-based simulated $\delta^{13}C$ was higher (Figures 9d,
434 S11d). Both temperature and RH modified tree-ring $\delta^{13}C$, especially in dry years when
435 climate-based simulations ($r = 0.38$) were similar to the observed $\delta^{13}C$ profiles (Figures
436 9c, 9e, S11c, S11e). However, climate modified $\delta^{13}C$ values less in wet years compare
437 to dry years (Figures 9d, 9f, S11d, S11f).

3.4 Conceptual model of intra-annual tree-ring $\delta^{13}C$ and $\delta^{18}O$ profiles

Combining climate responses and intra-annual profiles, we propose a conceptual model of intra-annul $\delta^{13}C$ and $\delta^{18}O$ profiles in dry versus wet years to interpret the intra-annual $\delta^{13}C$ and $\delta^{18}O$ and to illustrate how the leaf-water enrichment signal is transferred to the ring during the growing season in a subtropical humid site (Figure 10). We considered that: 1) tree-ring $\delta^{13}C$ is predominantly determined by stomatal control in dry years (more drought stress), but by photosynthetic rate in wet years; 2) the intra-annual tree-ring $\delta^{18}O$ profile is more altered in dry years compared to wet years (Figure 8e, 8f); 3) minimum tree-ring $\delta^{18}O$ occurs earlier in dry years compared to wet years.

4. Discussion

4.1 Climatic response in intra-annual tree-ring $\delta^{13}C$ and $\delta^{18}O$

Interannual variability in both thin-sectioned EW $\delta^{13}C_{cor}$ and EW $\delta^{18}O$ were affected by climate at the end of the prior dry season (October-November) (Figures 4, 5), along with strong relationships between LW $\delta^{13}C_{cor}$ of the previous year and EW $\delta^{13}C_{cor}$ of the current year (Figure S4d), suggesting climatic legacy effects (Castagneri *et al.*, 2018, Timofeeva *et al.*, 2017, Treydte *et al.*, 2014, Gessler *et al.*, 2013, Kagawa *et al.*, 2006). Legacy effects recorded in tree-ring $\delta^{13}C$ in pine may be caused by the use of stored carbohydrates or remobilization of starch from the previous year in constructing current year EW cell walls (Castagneri *et al.*, 2018, Timofeeva *et al.*, 2017,

458 Schubert & Jahren, 2011, Offermann *et al.*, 2011, Ogée et al., 2009, Kagawa *et al.*,
459 2006), and therefore tree-ring $\delta^{13}C$ may record previous year's climate conditions (Xu
460 *et al.*, 2020b, Szejner *et al.*, 2018, Timofeeva *et al.*, 2017). One of the mechanisms
461 responsible for the EW $\delta^{18}O$ reflecting previous year climate is the uptake by trees of
462 soil water that contains precipitation from previous seasons (Allen *et al.*, 2019, Treydte
463 *et al.*, 2014). Another possibility is that sugars from the previous year were used to build
464 leaf and xylem in the early growing season (Gessler *et al.*, 2013).

465 Interannual variability in LW $\delta^{18}O$ was driven primarily by RH in the current
466 growth year, particularly from August to October (Figure 4). At our site, trees might
467 suffer drought stress during this relatively dry period (Figure 1), which would strongly
468 determine the enrichments of soil-water $\delta^{18}O$ and leaf-water $\delta^{18}O$, compared to early
469 summer (Figures 2d, 8b). As a result, LW $\delta^{18}O$ values increased with SSD, EVP, and
470 VPD from August to October, but decreased with PRE and RH (Figure 4). Increased
471 ^{18}O in leaf water leads to heavier tree-ring $\delta^{18}O$ during dry conditions (i.e., low RH and
472 PRE) (Treydte *et al.*, 2014, Gessler *et al.*, 2013, Kahmen *et al.*, 2011).

473 Interannual variability in tree-ring $\delta^{13}C_{cor}$ in all EW and LW sections of the ring
474 increased with warming and decreased with higher RH and precipitation during the
475 growing season (Figure 5). During EW formation in the early growing season
476 (February-March), RH is relatively high, resulting in low stomatal limitation and low
477 EW $\delta^{13}C_{cor}$, which in turn is positively correlated with February-May temperature
478 (Figure 5). This evidence along with the positive (r = 0.2 - 0.5, $p < 0.05$) relationships

between LW $\delta^{13}C_{cor}$ and LW $\delta^{18}O$ (Figure S12), as well as significant correlations between LW $\delta^{13}C_{cor}$ and RH and VPD in September and October (Figure 5), suggest that LW $\delta^{13}C_{cor}$ was more influenced by stomatal conductance compared to EW $\delta^{13}C_{cor}$ (Farquhar *et al.*, 1982, Roden and Farquhar 2012, Scheidegger *et al.*, 2000). Low RH (high VPD) causes hydraulic stress on the trees and this leads to a reduction in stomatal conductance and therefore a decrease in C_i (Farquhar et al., 1982). In the dry late-growing season, high temperatures may enhance drought stress, which can in turn reduce stomatal conductance and therefore lead to reduced C_i/C_a and high $\delta^{13}C$ values (Scheidegger *et al.*, 2000, Farquhar *et al.*, 1982).

4.2 Intra-annual tree-ring $\delta^{13}C$ and $\delta^{18}O$ profiles and their drivers revealed by observations and models

The V-shaped intra-annual $\delta^{18}O$ profile in *Pinus massoniana* tracked the profile of growing season precipitation $\delta^{18}O$ (Figure 2), which was confirmed by our tree-ring $\delta^{18}O$ model simulations in wet years (Figure 8d, 8f), and agrees with results in other Asian monsoon areas (Zhu *et al.*, 2012a, Xu *et al.*, 2016). *Pinus massoniana* is known to mainly use superficial soil water (Yang *et al.*, 2015) and its intra-annual tree-ring $\delta^{18}O$ profile therefore reflects the profile of precipitation $\delta^{18}O$ throughout the growing season in humid conditions (Allen *et al.*, 2019).

On the other hand, $\delta^{18}O$ leaf-level enrichment can change the intra-annual tree-ring $\delta^{18}O$ profile (Roden *et al.*, 2000, Treydte *et al.*, 2014). Precipitation and RH

differences between wet and dry years did not lead to significant differences in growing-season precipitation $\delta^{18}O$ (Figures S7, S8). This suggests that source water $\delta^{18}O$ alone cannot cause differences in intra-annual tree-ring $\delta^{18}O$ profiles between wet and dry years, which is further confirmed by simulations based on source water $\delta^{18}O$ (Figure 8c-f). Compared to wet years, during dry years, a 6% (0.1% to 14%) decrease in growing-season RH (Figure S7) leads to a 2.4‰ (0.04‰ to 5.9‰) increase in the ^{18}O enrichment at the leaf level. This translates into about 1.4‰ (0.02‰ to 3.4‰) increase in tree-ring cellulose $\delta^{18}O$ assuming $P_{ex} \approx 42\%$ in the Roden model (Roden *et al.*, 2000). These magnitudes are comparable with the differences observed in tree-ring $\delta^{18}O$ between dry and wet years (Figure 6a).

Intra-annual tree-ring $\delta^{18}O$ shows a flat profile in dry years and a distinct V-shaped profile in wet years (Figure 6). In wet years, high RH leads to low leaf-level enrichment, especially for EW $\delta^{18}O$, and intra-annual tree-ring $\delta^{18}O$ profiles predominantly follow precipitation $\delta^{18}O$ profiles with a distinct "V" pattern (Figures 6b, 8d, 8f). In dry years, however, trees are faced with limited water availability, particularly low RH, and tree-ring $\delta^{18}O$ was strongly modified by leaf-level enrichment (Barbour *et al.*, 2004, Treydte *et al.*, 2014, Belmecheri *et al.*, 2018, Roden *et al.*, 2000), resulting in higher tree-ring $\delta^{18}O$ values with lower variability and a flat V-shape profile compared to wet years (Figures 6, 8c, 8e). This explanation can be further supported by our model results that show that in dry years, the enrichment-based simulation better captured the tree-ring $\delta^{18}O$ profile than other simulations (Figure 8). Furthermore, minimum $\delta^{18}O$ can be

considered a biomarker for low $\delta^{18}O$ in precipitation and/or low leaf-$\delta^{18}O$ enrichment in monsoonal Asia (Zhu *et al.*, 2012b, Xu *et al.*, 2020a). Considering that precipitation $\delta^{18}O$ in June-July-August does not differ significantly between dry and wet years (Figure 6c), the stronger and earlier leaf-level $\delta^{18}O$ enrichment in dry years leads to a higher probability of minima $\delta^{18}O$ in EW and late-LW compared to wet years (Figures 6, 8). In addition to this, the later tree-ring $\delta^{18}O$ minimum in wet years may be associated with higher RH and higher PRE in the late growing season (August-October) compared to dry years (Figures S7). Similarly, the transition from EW to LW usually occurs earlier in dry years compared to wet years (Gruber *et al.*, 2010).

The Roden full model prominent overestimated intra-annual tree-ring $\delta^{18}O$ profiles during dry years (Figure 8c), which contradicts our hypothesis that the model will be more accurate in dry years. This larger decoupling in dry years may result from 1) larger evaporative enrichment effects or the residence time in precipitation $\delta^{18}O$ variability (Gessler *et al.*, 2014, Treydte *et al.*, 2014), 2) differences between air and leaf temperature in dry years (low RH), with leaf temperature typically lower than air temperature, resulting in leaf-enrichment overestimation, and 3) influences of post-photosynthetic processes, such as assimilates storage and remobilization processes (Timofeeva *et al.*, 2017, Offermann *et al.*, 2011). These processes may dampen the variance of the source-water $\delta^{18}O$ and result in a lack of short-term signals (i.e., week-to-week variability in tree-ring $\delta^{18}O$) (Gessler *et al.*, 2014, Treydte *et al.*, 2014) and low variability in observed intra-annual tree-ring $\delta^{18}O$ profiles (Figure 8c).

The asymmetrical inverse-V-shaped intra-annual $\delta^{13}C$ profile followed atmospheric $\delta^{13}C$ changes and VPD (Figures 3, 9). Tree-ring $\delta^{13}C$ showed a lower value at the start and end of the tree ring compared to the middle sections, as has been described for other pine species (Fonti *et al.*, 2018, Sarris *et al.*, 2013). Tree-ring $\delta^{13}C$ is mainly determined by the high photosynthetic rate in April-May because stomatal control does not impose limitations in wet spring (low VPD; Figure 1c), and therefore assimilates are depleted in $\delta^{13}C$. The tree-ring $\delta^{13}C$ peak may be caused by high VPD (2.8-3.4 hPa in July-August), which leads to lower C_i/C_a compared to spring (Boyer & Kawamitsu, 2011, Jarman, 1974).

We found reverse intra-annual profiles in wet versus dry years for tree-ring $\delta^{13}C$ compared to $\delta^{18}O$, with $\delta^{13}C$ showing a fairly constant intra-annual profile in wet years (Figures 7, 9), but steeper slopes from EW to the late LW in dry years. This increase in $\delta^{13}C$ towards the late LW (LW2-5) in dry years can be attributed to a reduction in stomatal conductance because RH decreases and $\delta^{18}O$ increase from middle to LW in dry years (Figures 1, 6c) according to the dual-isotope model (Roden and Farquhar 2012, Scheidegger *et al.*, 2000). EW $\delta^{13}C$ values showed a constant offset (0.4‰) between wet and dry years (Figures 7b, 9), which evidences that stomatal conductance does not change profile pattern in EW. In the late-growing season, on the other hand, stomatal conductance strongly responded to low RH in dry years (Figure 9c) and resulted in enriched $\delta^{13}C$ in leaf and LW (Farquhar *et al.*, 1982). As a result, LW $\delta^{13}C$ simulations based on climate followed the observed profiles, especially in dry years

(Figures 9c, 9e, S11c), suggesting the strong influence of temperature and moisture (i.e, precipitation and RH), as well as their interactions.

Farquhar-modeled intra-annual $\delta^{13}C$ profiles were more similar to observations in dry years, especially for simulations based on full, climate, and RH models (Figure 9c, 9e), but $\delta^{13}C$ profiles showed a larger divergence between these simulations and observations in wet years compared to dry years (Figure 9e, 9f). This divergence may be due to an overestimation of the contribution of climate (Figure 9c, 9d). The divergence (0.05~0.2‰) between simulated and measured $\delta^{13}C$ in the early EW may result from different cambial activity onsets, legacy effects, and photosynthetic rates (Fonti *et al.*, 2018, Huang *et al.*, 2018, Offermann *et al.*, 2011).

The differences in intra-annual $\delta^{18}O$ and $\delta^{13}C$ profiles in dry and wet years suggest different predominant ecophysiological controls. As a result, separate interpretations of intra-annual $\delta^{18}O$ and $\delta^{13}C$ profiles in wet and dry years are needed in humid environments in general and at our site specifically.

4.3 Conceptual model of intra-annual eco-physiological responses to dry and wet conditions

Conceptual tree-ring $\delta^{18}O$ models exist for the tropics at the seasonal scale (Schubert & Jahren, 2015, Managave & Ramesh, 2012, Evans & Schrag, 2004), but they do not consider intra-annual profiles or tree-ring $\delta^{13}C$. Our conceptual model (Figure 10) considers not only these factors, but also the position of the $\delta^{18}O$ minimum

582 and provides a new perspective to interpret intra-annual tree-ring $\delta^{13}C$ and $\delta^{18}O$ profiles
583 separately.

584 In our conceptual model, the main mechanisms involved stomatal and
585 photosynthetic rate controls are dynamic and complex and differ for different tree-ring
586 sections: in dry years, due to drought stress, stomatal control overrides the control
587 exerted by the photosynthetic rate at the beginning of the growing season, but at the end
588 of the growing season stomatal control is reduced and goes to a new balance with the
589 photosynthetic rate (Figure 10). On the other hand, stomatal control is balanced with
590 photosynthetic rate at beginning of the growing season in wet years. Then, because of
591 low drought stress, photosynthetic rate dominates the $\delta^{13}C$ value until the
592 photosynthetic rate reaches a maximum value. At the end of the growing season, the
593 photosynthetic rate decreases again and reaches a new balance with stomatal control
594 (Figure 10).

595 By comparing Roden model simulations with our observations in wet and dry
596 years (Figure 8), we found that the intra-annual tree-ring $\delta^{18}O$ profile follows the
597 precipitation $\delta^{18}O$ profile in wet years, but in dry years leaf-water enrichment dominates
598 the tree-ring $\delta^{18}O$ and alters the profile (Figure 8c), resulting in higher tree-ring $\delta^{18}O$
599 values from the end of EW to the end of LW. The strongest influence of leaf-water
600 enrichment thus happens in the central part of the transition between EW and LW, when
601 tree-ring $\delta^{18}O$ shows the largest divergence between dry and wet years (Figures 6, S9).

602 Our model indicates a stronger stomatal limitation on $\delta^{13}C$ during the formation

603 of the early-LW compared to the period of EW formation, especially in dry years. Intra-
604 annual $\delta^{13}C$ profile variability was larger in dry years due to high LW $\delta^{13}C$ values
605 caused by strong water limitation and a lower stomatal conductance (Roussel *et al.*,
606 2009). Our conceptual $\delta^{13}C$ model suggests a plastic physiological response to drought
607 throughout the growing season reflected in different tree-ring sections. Intra-annual
608 $\delta^{13}C$ variability is thus strongly related to stomatal control, particularly in the central
609 and early-LW sections. Therefore, in a broader view, these sections of the tree ring are
610 a better choice compared to the whole ring when exploring long-term drought responses
611 and vegetation-climate interactions under increasing VPD scenarios (Kahmen *et al.*,
612 2011).

613 Leaf water enrichment impacted the intra-annual $\delta^{18}O$ profile, especially in dry
614 years (Figure 8). Decreasing RH (Figures 1, 8) and increasing VPD (Monson *et al.*,
615 2018, Belmecheri *et al.*, 2018, Szejner et al., 2021) changed the intra-annual $\delta^{18}O$
616 profile by altering the intra-annual V-shape profile of the source-water $\delta^{18}O$. In wet
617 years, on the other hand, the intra-annual tree-ring $\delta^{18}O$ profile tracked the precipitation
618 $\delta^{18}O$ profile. In the monsoon region, $\delta^{18}O$ from different sections of the tree ring may
619 have varied climate signals (Xu *et al.*, 2020a, Zhu *et al.*, 2012b, An *et al.*, 2012). Our
620 results confirm this and the conceptual model further suggests that the EW-LW
621 transition sections can be a better target when using $\delta^{13}C$ to track drought responses and
622 when using tree-ring $\delta^{18}O$ to track climatic signal and precipitation $\delta^{18}O$. Again, our
623 conceptual model illustrates the interplay of mechanisms governing tree-ring stable

isotopes within the ring, which helps extract stronger climatic signals using potential concrete sections of the tree ring and study the trade-off between source-water $\delta^{18}O$ and leaf-water enrichment (Allen *et al.*, 2019, Szejner *et al.*, 2018).

5. Conclusion

We analyzed intra-annual tree-ring $\delta^{13}C$ and $\delta^{18}O$ profiles and their interannual variability, as well as their driving mechanisms. We found that interannual $\delta^{18}O$ variability is related to moisture availability and its intra-annual profile tracks precipitation $\delta^{18}O$ variations. Interannual $\delta^{13}C$ variability, on the other hand, is mainly determined by early growing season (February-May) temperature and late growing season (September-October) moisture. The intra-annual $\delta^{18}O$ profile showed larger variability following the magnitude of source water seasonal variations and delayed within-season minima in wet years compared to dry years, because there is a little evaporative leaf-level isotopic enrichment during wet years. The intra-annual $\delta^{13}C$ profiles showed lower mean values and flatter slopes during wet years compared to dry years.

The Roden process-based model shows skill in capturing intra-annual $\delta^{18}O$ profiles in wet years, but not in dry years, which suggests that the process-based model shows some asymmetric bias in reproducing the difference in the dominant mechanistic processes in dry versus wet years, such as source-water $\delta^{18}O$ signal and leaf-level enrichment controls. On the other hand, the Farquhar-model captured $\delta^{13}C$ better in dry

years compared to wet years. This model outcome can be explained by differences in the controlling factors on ecophysiological processes and tree growth between dry (strong stomatal control) and wet (low stomatal control) years. We thus provided an intra-annual conceptual model to interpret intra-annual tree-ring $\delta^{13}C$ and $\delta^{18}O$ profiles in wet and dry years considering climate response, isotopic source, and ecophysiological mechanisms.

Acknowledgments

We thank Dr. Soumaya Belmecheri for providing the code of the Roden model and Dr. Kei Yoshimura for providing the IsoGSM model outputs. We thank Drs. Xuanwen Zhang, Guoju Wu, Bo Wang, and Mrs. Weizhen Sun for stable isotope measurements. This research was funded by the National Natural Science Foundation of China (41871030, 4172109& 41971104), by the Self-determination Project of the State Key Laboratory of Cryospheric Sciences (SKLCS-ZZ-2021), by the Youth Innovation Promotion Association, CAS (2016372), and by funding from the Chinese Scholarship Council (201704910171). ID-L received financial support from Fundació La Caixa through the Junior Leader Program (LCF/BQ/LR18/11640004).

Data availability statement

Data and code in this study can be found in https://github.com/GuobaoXu/Intral-annual-tree-ring-stable-isotope after publication. The meteorological data can be downloaded from http://data.cma.cn/en by registration. The Changsha station

precipitation $\delta^{18}O$ can be found in the GNIP database (https://www.iaea.org/services/networks/gnip).

Author contributions

GBX, XHL, TC, and VT provided the ideas and designed the methodology; GBX, VT, and XHL analyzed the data; GBX, VT, and ID-L led the writing of the manuscript; JH, MG, XHL, PS, and TC helped to interpret data and to improve the drafts.

References

Anchukaitis K.J. & Evans M.N. (2010) Tropical cloud forest climate variability and the demise of the Monteverde golden toad. *Proceedings of the National Academy of Sciences ,107*, 5036–5040. https://doi.org/10.1073/pnas.0908572107

Allen S.T., Kirchner J.W., Braun S., Siegwolf R.T.W. & Goldsmith G.R. (2019) Seasonal origins of soil water used by trees. *Hydrology and Earth System Sciences*, *23*, 1199-1210.

An W., Liu X., Leavitt S.W., Ren J., Sun W., Wang W., Wang Y., Xu G., Chen T. & Qin D. (2012) Specific climatic signals recorded in earlywood and latewood $\delta^{18}O$ of tree rings in southwestern China. *Tellus B*, *64*, 18703.

Andreu-Hayles L., Levesque M., Martin-Benito D., Huang W., Harris R., Oelkers R., Leland C., Martin-Fernández J., Anchukaitis K.J. & Helle G. (2018) A high yield cellulose extraction system for small whole wood samples and dual measurement of carbon and oxygen stable isotopes. *Chemical Geology*, *504*, 53-65.

Barbour M.M., Roden J.S., Farquhar G.D. & Ehleringer J.R. (2004) Expressing leaf water and cellulose oxygen isotope ratios as enrichment above source water reveals evidence of a Péclet effect. *Oecologia*, *138*, 426-435.

Belmecheri S., Wright W.E., Szejner P., Morino K.A. & Monson R.K. (2018) Carbon and oxygen isotope fractionations in tree rings reveal interactions between cambial

phenology and seasonal climate. *Plant, Cell and Environment, 41*, 2758-2772.

Belmecheri S. & Lavergne A. (2020) Compiled records of atmospheric CO2 concentrations and stable carbon isotopes to reconstruct climate and derive plant ecophysiological indices from tree rings. *Dendrochronologia, 63*.

Belmecheri et al. (2022). In: *Stable isotopes in Tree rings: Inferring Physiological, Climatic and Environmental Responses* (ed Siegwolf R. T. W.), Springer Berlin Heidelberg, Berlin, Heidelberg.. https://link.springer.com/book/9783030926977

Berkelhammer M. & Stott L.D. (2009) Modeled and observed intra-ring $\delta^{18}O$ cycles within late Holocene Bristlecone Pine tree samples. *Chemical Geology, 264*, 13-23.

Bolton D. (1980) The computation of equivalent potential temperature. *Monthly Weather Review, 108*, 1046-1053.

Boyer J.S. & Kawamitsu Y. (2011) Photosynthesis gas exchange system with internal CO2 directly measured. *Environmental Control in Biology, 49*, 193-207.

Bunn A.G. (2010) Statistical and visual crossdating in R using the dplR library. *Dendrochronologia, 28*, 251-258.

Castagneri D., Battipaglia G., von Arx G., Pacheco A. & Carrer M. (2018) Tree-ring anatomy and carbon isotope ratio show both direct and legacy effects of climate on bimodal xylem formation in *Pinus pinea*. *Tree Physiology, 38*, 1098-1109.

Cernusak L.A., Barbour M.M., Arndt S.K., Cheesman A.W., English N.B., Feild T.S., Helliker B.R., Holloway-Phillips M.M., Holtum J.A., Kahmen A., McInerney F.A., Munksgaard N.C., Simonin K.A., Song X., Stuart-Williams H., West J.B. & Farquhar G.D. (2016) Stable isotopes in leaf water of terrestrial plants. *Plant, Cell and Environment, 39*, 1087-1102.

Cheesman A.W. & Cernusak L.A. (2017) Infidelity in the outback: climate signal recorded in $\Delta^{18}O$ of leaf but not branch cellulose of eucalypts across an Australian aridity gradient. *Tree Physiology,* 37, 554-564.

716 Cook E.R. & Kairiukstis L.A. (1990) *Methods of dendrochronology: applications in*
717 *the environmental sciences*. Kluwer Academic Publishers, Boston.
718 Dansgaard W. (1964) Stable isotopes in precipitation. *Tellus, 16*, 436-468.
719 Ding Y. & Chan J.C.L. (2005) The East Asian summer monsoon: an overview.
720 *Meteorology and Atmospheric Physics, 89*, 117-142.
721 DeSoto L., De la Cruz M. & Fonti P. (2011). Intra-annual patterns of tracheid size in
722 the Mediterranean tree *Juniperus thurifera* as an indicator of seasonal water stress.
723 *Canadian Journal of Forest Research,* 41, 1280-1294
724 Evans M.N. & Schrag D.P. (2004) A stable isotope-based approach to tropical
725 dendroclimatology. *Geochimica et Cosmochimica Acta, 68*, 3295-3305.
726 Evans M.N., Selmer K.J., Breeden III B.T., Lopatka A.S. & Plummer R.E. (2016)
727 Correction algorithm for online continuous flow $\delta^{13}C$ and $\delta^{18}O$ carbonate and
728 cellulose stable isotope analyses. *Geochemistry, Geophysics, Geosystems, 17*,
729 3580-3588.
730 Farquhar G.D., O'Leary M.H. & Berry J.A. (1982) On the relationship between carbon
731 isotope discrimination and the intercellular carbon dioxide concentration in leaves.
732 *Australian Journal of Plant Physiology, 9*, 121-137.
733 Farquhar G.D. & Lloyd J. (1993) Carbon and Oxygen Isotope Effects in the Exchange
734 of Carbon Dioxide between Terrestrial Plants and the Atmosphere. In: *Stable*
735 *Isotopes and Plant Carbon-water Relations* (eds J.R. Ehleringer, A.E. Hall, & G.D.
736 Farquhar), pp. 47-70. Academic Press, San Diego.
737 Fonti M.V., Vaganov E.A., Wirth C., Shashkin A.V., Astrakhantseva N.V. & Schulze
738 E.D. (2018) Age-effect on intra-annual $\delta^{13}C$-variability within Scots Pine tree-
739 rings from Central Siberia. *Forests, 9*, 364.
740 Gessler A., Brandes E., Keitel C., Boda S., Kayler Z.E., Granier A., Barbour M.,
741 Farquhar G.D. & Treydte K. (2013) The oxygen isotope enrichment of leaf-
742 exported assimilates - does it always reflect lamina leaf water enrichment? *New*

Phytologist, *200*, 144-157.

Gessler A., Ferrio J.P., Hommel R., Treydte K., Werner R.A. & Monson R.K. (2014) Stable isotopes in tree rings: towards a mechanistic understanding of isotope fractionation and mixing processes from the leaves to the wood. *Tree Physiology*, *34*, 796-818.

Gruber A., Strobl S., Veit B. & Oberhuber W. (2010) Impact of drought on the temporal dynamics of wood formation in Pinus sylvestris. *Tree Physiology*, *30*, 490-501.

Helle G. & Schleser G.H. (2004) Beyond CO_2-fixation by Rubisco – an interpretation of $^{13}C/^{12}C$ variations in tree rings from novel intra-seasonal studies on broad-leaf trees. *Plant, Cell and Environment*, *27*, 367–380.

Huang J., Guo X., Rossi S., Zhai L., Yu B., Zhang S. & Zhang M. (2018) Intra-annual wood formation of subtropical Chinese red pine shows better growth in dry season than wet season. *Tree Physiology*, *38*, 1225-1236.

Huang J.G., Ma Q., Rossi S., Biondi F., Deslauriers A., Fonti P. *et al.* (2020) Photoperiod and temperature as dominant environmental drivers triggering secondary growth resumption in Northern Hemisphere conifers. *Proceedings of the National Academy of Sciences*, 117:20645-20652.

Jarman P. (1974) The diffusion of carbon dioxide and water vapour through stomata. *Journal of Experimental Botany*, *25*, 927-936.

Kagawa A., Sugimoto A. & Maximov T.C. (2006) Seasonal course of translocation, storage and remobilization of ^{13}C pulse-labeled photoassimilate in naturally growing *Larix gmelinii* saplings. *New Phytologist*, *171*, 793-804.

Kahmen A., Sachse D., Arndt S.K., Tu K.P., Farrington H., Vitousek P.M. & Dawson T.E. (2011) Cellulose $\delta^{18}O$ is an index of leaf-to-air vapor pressure difference (VPD) in tropical plants. *Proceedings of the National Academy of Sciences*, *108*, 1981-1986.

Lavergne A., Gennaretti F., Risi C., Daux V., Boucher E., Savard M.M., Naulier M.,

770 Villalba R., Bégin C. & Guiot J. (2017) Modelling tree ring cellulose $\delta^{18}O$
771 variations in two temperature-sensitive tree species from North and South America.
772 *Climate of the Past, 13*, 1515-1526.
773 Liñán I. D., Gutiérrez E., Helle G., Heinrich I., Andreu-Hayles L., Planells O.,
774 Leuenberger M., Burger C. & Schleser G. (2011). Pooled versus separate
775 measurements of tree-ring stable isotopes. *Science of the Total Environment,*
776 *409*(11), 2244-2251. doi:10.1016/j.scitotenv.2011.02.010
777 Leavitt S.W. & Danzer S.R. (1993) Method for batch processing small wood samples
778 to holocellulose for stable-carbon isotope analysis. *Analytical Chemistry, 65*, 87-
779 89.
780 Loader N.J., Robertson I., Barker A.C., Switsur V.R. & Waterhouse J.S. (1997) An
781 improved technique for the batch processing of small wholewood samples to α-
782 cellulose. *Chemical Geology, 136*, 313-317.
783 Loader N.J., Street-Perrott F.A., Daley T.J., Hughes P.D.M., Kimak A., Levanič T.,
784 Mallon G., Mauquoy D., Robertson I., Roland T.P., van Bellen S., Ziehmer M.M.
785 & Leuenberger M. (2014) Simultaneous Determination of Stable Carbon, Oxygen,
786 and Hydrogen Isotopes in Cellulose. *Analytical Chemistry*, *87*, 376-380.
787 Managave S.R. & Ramesh R. (2012) Isotope Dendroclimatology: A Review with a
788 Special Emphasis on Tropics. In: *Handbook of Environmental Isotope*
789 *Geochemistry: Vol I* (ed M. Baskaran), pp. 811-833. Springer Berlin Heidelberg,
790 Berlin, Heidelberg.
791 McCarroll D. & Loader N.J. (2004) Stable isotopes in tree rings. *Quaternary Science*
792 *Reviews*, *23*, 771-801.
793 McDowell N., Allen C.D. & Marshall L. (2010) Growth, carbon-isotope discrimination,
794 and drought-associated mortality across a *Pinus ponderosa* elevational transect.
795 *Global Change Biology, 16*, 399-415.
796 Monson R.K., Szejner P., Belmecheri S., Morino K.A. & Wright W.E. (2018) Finding

797 the seasons in tree ring stable isotope ratios. *American Journal of Botany*, *105*,
798 819-821.
799 Ogée, J., M. Barbour, L. Wingate, D. Bert, A. Bosc, M. Stievenard, C. Lambrot, M.
800 Pierre, T. Bariac & D. Loustau. 2009. A single-substrate model to interpret intra-
801 annual stable isotope signals in tree-ring cellulose. *Plant, Cell and Environment*
802 32,1071-1090.
803 Offermann C., Ferrio J.P., Holst J., Grote R., Siegwolf R., Kayler Z. & Gessler A. (2011)
804 The long way down—are carbon and oxygen isotope signals in the tree ring
805 uncoupled from canopy physiological processes? *Tree Physiology*, *31*, 1088-1102.
806 Rinne K.T., Saurer M., Kirdyanov A.V., Loader N.J., Bryukhanova M.V., Werner R.A.
807 & Siegwolf R.T.W. (2015) The relationship between needle sugar carbon isotope
808 ratios and tree rings of larch in Siberia. *Tree Physiology*, *35*, 1192-1205.
809 Roden J. & Siegwolf R. (2012) Is the dual-isotope conceptual model fully operational?
810 *Tree Physiology*, *32*, 1179-1182.
811 Roden J.S., Lin G. & Ehleringer J.R. (2000) A mechanistic model for interpretation of
812 hydrogen and oxygen isotope ratios in tree-ring cellulose. *Geochimica et*
813 *Cosmochimica Acta*, *64*, 21-35.
814 Roden, J. S., & G. D. Farquhar. (2012) A controlled test of the dual-isotope approach
815 for the interpretation of stable carbon and oxygen isotope ratio variation in tree
816 rings. Tree Physiology **32**:490-503.
817 Rossi, S., Morin, H., & Deslauriers, A. (2012). Causes and correlations in cambium
818 phenology: Towards an integrated framework of xylogenesis. *Journal of*
819 *Experimental Botany*, 63, 2117–2126.
820 Roussel M., Dreyer E., Montpied P., Le-Provost G., Guehl J.M. & Brendel O. (2009)
821 The diversity of (13)C isotope discrimination in a Quercus robur full-sib family is
822 associated with differences in intrinsic water use efficiency, transpiration
823 efficiency, and stomatal conductance. *Journal of Experimental Botany*, *60*, 2419-

2431.

Sarris D., Siegwolf R. & Korner C. (2013) Inter- and intra-annual stable carbon and oxygen isotope signals in response to drought in Mediterranean pines. *Agricultural and Forest Meteorology*, *168*, 59-68.

Scheidegger Y., Saurer M., Bahn M. & Siegwolf R. (2000) Linking stable oxygen and carbon isotopes with stomatal conductance and photosynthetic capacity: a conceptual model. *Oecologia*, *125*, 350-357.

Schollaen K., Heinrich I. & Helle G. (2014) UV-laser-based microscopic dissection of tree rings - a novel sampling tool for $\delta^{13}C$ and $\delta^{18}O$ studies. *New Phytologist*, *201*, 1045-1055.

Schubert B.A. & Jahren A.H. (2011). Quantifying seasonal precipitation using high-resolution carbon isotope analyses in evergreen wood. *Geochimica et Cosmochimica Acta*, 75, 7291-7303.

Schubert B.A. & Jahren A.H. (2015) Seasonal temperature and precipitation recorded in the intra-annual oxygen isotope pattern of meteoric water and tree-ring cellulose. *Quaternary Science Reviews*, 125, 1-14.

Schubert B.A. & Timmermann, A. (2015) Reconstruction of seasonal precipitation in Hawai'i using high-resolution carbon isotope measurements across tree rings. Chemical Geology, 417, 273-278.

van der Sleen P., Zuidema P.A., Pons T.L. & Oliveira R. (2017) Stable isotopes in tropical tree rings: theory, methods and applications. *Functional Ecology*, 31, 1674-1689.

Sohn J.A., Kohler M., Gessler A. & Bauhus J. (2012) Interactions of thinning and stem height on the drought response of radial stem growth and isotopic composition of Norway spruce (*Picea abies*). *Tree Physiology*, *32*, 1199-1213.

Song X., Clark K.S. & Helliker B.R. (2014) Interpreting species-specific variation in tree-ring oxygen isotope ratios among three temperate forest trees. *Plant Cell and*

Environment, *37*, 2169-2182.

Sternberg L.S.L.O.R. (2009) Oxygen stable isotope ratios of tree-ring cellulose: the next phase of understanding. *New Phytologist*, *181*, 553-562.

Szejner P., Wright W.E., Belmecheri S., Meko D., Leavitt S.W., Ehleringer J.R. & Monson R.K. (2018) Disentangling seasonal and interannual legacies from inferred patterns of forest water and carbon cycling using tree-ring stable isotopes. *Global Change Biology*, *24*, 5332-5347.

Szejner, P., Belmecheri, S., Ehleringer, J. R., & Monson, R. K. (2020a). Recent increases in drought frequency cause observed multi-year drought legacies in the tree rings of semi-arid forests. *Oecologia*, *192*(1), 241-259. doi:10.1007/s00442-019-04550-6

Szejner P., Clute T., Anderson E., Evans M.N. & Hu J. (2020b) Reduction in lumen area is associated with the $\delta^{18}O$ exchange between sugars and source water during cellulose synthesis. *New Phytologist*, *226*, 1583-1593.

Szejner P, Belmecheri S, Babst F, Wright WE, Frank C, Hu J, Monson RK. (2021) Stable isotopes of tree rings reveal seasonal-to-decadal patterns during the emergence of a megadrought in the Southwestern US. *Oecologia*, *197*, 1079–1094. https://doi.org/10.1007/s00442-021-04916-9

Timofeeva G., Treydte K., Bugmann H., Rigling A., Schaub M., Siegwolf R. & Saurer M. (2017) Long-term effects of drought on tree-ring growth and carbon isotope variability in Scots pine in a dry environment. *Tree Physiology*, *37*, 1028-1041.

Treydte K., Boda S., Graf Pannatier E., Fonti P., Frank D., Ullrich B., Saurer M., Siegwolf R., Battipaglia G., Werner W. & Gessler A. (2014) Seasonal transfer of oxygen isotopes from precipitation and soil to the tree ring: source water versus needle water enrichment. *New Phytologist*, *202*, 772-783.

Vaganov E. (1990) The tracheidogram method in tree-ring analysis and its application. *Methods of dendrochronology*, *63*, 67.

878 Xu C., Zheng H., Nakatsuka T., Sano M., Li Z. & Ge J. (2016) Inter- and intra-annual
879 tree-ring cellulose oxygen isotope variability in response to precipitation in
880 Southeast China. *Trees-Structure and Function, 30*, 785-794.
881 Xu G., Liu X., Sun W., Chen T., Zhang X., Zeng X., Wu G., Wang W. & Qin D. (2018)
882 Application and verification of simultaneous determination of cellulose $\delta^{13}C$ and
883 $\delta^{18}O$ in *Picea shrenkiana* tree rings from northwestern China using the high-
884 temperature pyrolysis method. *Journal of Arid Land, 10*, 864–876.
885 Xu G., Liu X., Sun W., Szejner P., Zeng X., Yoshimura K. & Trouet V. (2020a) Seasonal
886 divergence between soil water availability and atmospheric moisture recorded in
887 intra-annual tree-ring $\delta^{18}O$ extremes. *Environmental Research Letters*. *15*, 094036.
888 Xu G., Wu G., Liu X., Chen T., Wang B., Hudson A. & Trouet V. (2020b) Age-related
889 climate response of tree-ring $\delta^{13}C$ and $\delta^{18}O$ from spruce in northwestern China,
890 with implications for relative humidity reconstructions. *Journal of Geophysical*
891 *Research: Biogeosciences*, *125*, e2019JG005513.
892 Yang B., Wen X. & Sun X. (2015) Seasonal variations in depth of water uptake for a
893 subtropical coniferous plantation subjected to drought in an East Asian monsoon
894 region. *Agricultural and Forest Meteorology, 201*, 218-228.
895 Yoshimura K. (2015) Stable water isotopes in climatology, meteorology, and hydrology:
896 A review. *Journal of the Meteorological Society of Japan, 93*, 513-533.
897 Zang C. & Biondi F. (2015) Treeclim: an R package for the numerical calibration of
898 proxy-climate relationships. *Ecography, 38*, 431-436.
899 Zeng X., Liu X., Treydte K., Evans M.N., Wang W., An W., Sun W., Xu G., Wu G. &
900 Zhang X. (2017) Climate signals in tree-ring $\delta^{18}O$ and $\delta^{13}C$ from southeastern
901 Tibet: insights from observations and forward modelling of intra- to interdecadal
902 variability. *New Phytologist, 216*, 1104-1118.
903 Zhang H. & Nobel P.S. (1996) Dependency of c_i/c_a and leaf transpiration efficiency on
904 the vapour pressure deficit. *Functional Plant Biology, 23*, 561-568.

905 Zhang S., Rossi S., Huang J., Jiang S., Yu B., Zhang W. & Ye Q. (2018) Intra-annual
906 dynamics of xylem formation in *Liquidambar formosana* subjected to canopy and
907 understory N addition. *Frontiers in Plant Science*, *9*, 79.
908 Zhu M., Stott L., Buckley B., Yoshimura K. & Ra K. (2012a) Indo-Pacific Warm Pool
909 convection and ENSO since 1867 derived from Cambodian pine tree cellulose
910 oxygen isotopes. *Journal of Geophysical Research*, *117*, D11307.
911 Zhu M.F., Stott L., Buckley B. & Yoshimura K. (2012b) 20th century seasonal moisture
912 balance in Southeast Asian montane forests from tree cellulose $\delta^{18}O$. *Climatic*
913 *Change*, *115*, 505-517.

914 **Table**

915 **Table 1** Model parameters designed to detect the contribution of each process or parameter.

916 The parameter values can be found in the supplemental table S2.

Model	model contributor	Input fixed parameter	Changing parameter	Constant parameters	Offset (‰)
Farquhar full Model	Full model	a, b, c1, c2, $offset_{pc}$	temperature, RH, $\delta^{13}C_{atm}$	/	/
Farquhar single parameter Model	Climate contri	a, b, c1, c2, $offset_{pc}$	temperature, RH	$\delta^{13}C_{atm}$	/
	RH contri	a, b, c1, c2, $offset_{pc}$	RH	$\delta^{13}C_{atm}$, temperature	/
	Tem contri	a, b, c1, c2, offset_pc	temperature	$\delta^{13}C_{atm}$, RH	/
	$\delta^{13}C_{atm}$ contri	a, b, c1, c2, $offset_{pc}$	$\delta^{13}C_{atm}$	temperature, RH	/
Roden full Model	Full model	ε_c, ε_k, ε^*, P_{ex}, g_b, g_s	$\delta^{18}O$ of precipitation, $\delta^{18}O$ of water vapor, RH, temperature	/	-0.09
Roden single parameter Model	Enrichment contri	ε_c, ε_k, ε^*, P_{ex}, g_b, g_s	RH, temperature	$\delta^{18}O$ of precipitation, $\delta^{18}O$ of water vapor	2.77
	Source water $\delta^{18}O$ contri	ε_c, ε_k, ε^*, P_{ex}, g_b, g_s	$\delta^{18}O$ of precipitation	RH, temperature	3.07

917

Figures and Figure captions

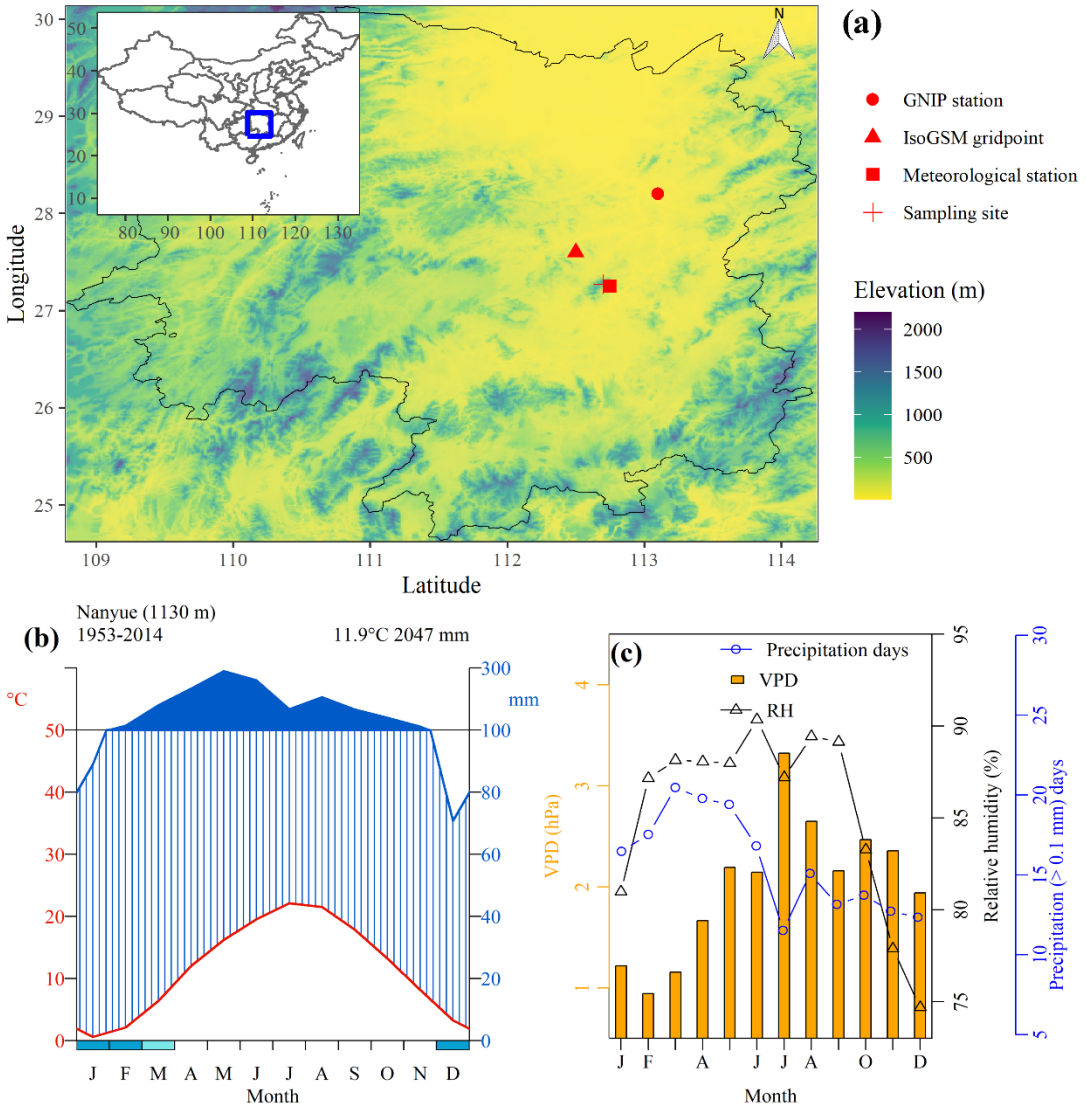

Figure 1 (a) Location of the sampling site, Nanyue weather station, and precipitation $\delta^{18}O$ (GNIP) station. (b) Walter and Lieth climatic diagram of the Nanyue station showing mean values for the period 1953-2014. The blue (red) line represents the mean monthly precipitation (mean air temperature). Blue shaded area indicates the wet period and vertical blue lines indicate the humid period. The dark (light) blue horizontal bars below the X-axis represent frost (likely frost) periods. (c) Monthly precipitation (> 0.1 mm) days, vapor pressure deficit (VPD), and relative humidity (RH).

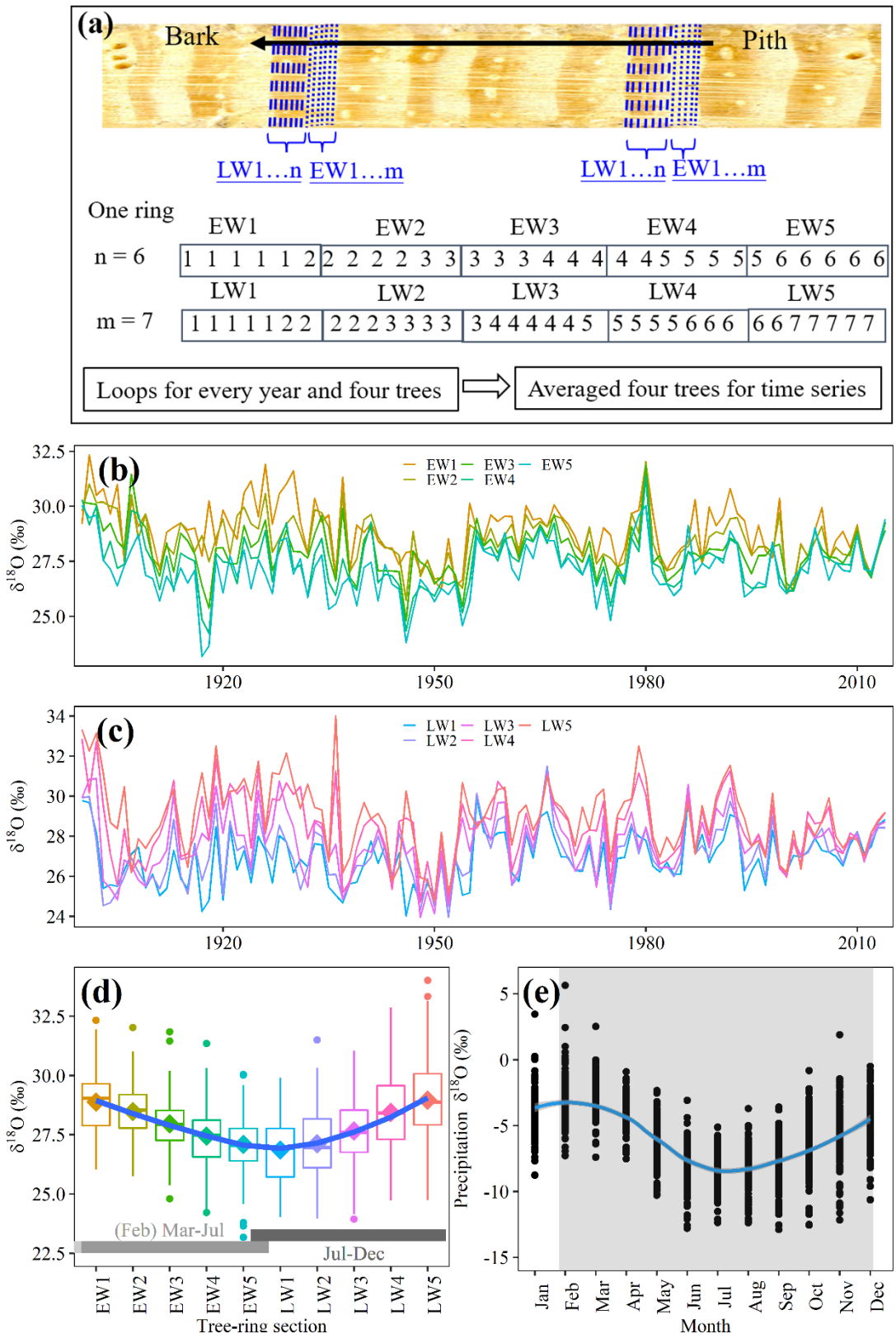
(a)
Bark
Pith
LW1…n EW1…m
LW1…n EW1…m
One ring
EW1 EW2 EW3 EW4 EW5
n = 6
1 1 1 1 1 2 2 2 2 2 3 3 3 3 3 4 4 4 4 4 5 5 5 5 5 5 6 6 6 6 6 6
LW1 LW2 LW3 LW4 LW5
m = 7
1 1 1 1 1 2 2 2 2 3 3 3 3 4 4 4 4 4 4 5 5 5 5 5 6 6 6 5 5 5 6 6 7 7 7 7 7
Loops for every year and four trees
Averaged four trees for time series
(b)
EW1 EW2 EW3 EW4 EW5
δ18O (‰)
32.5
30.0
27.5
25.0
1920
1950
1980
2010
(c)
LW1 LW2 LW3 LW4 LW5
δ18O (‰)
34
32
30
28
26
24
1920
1950
1980
2010
(d)
δ18O (‰)
32.5
30.0
27.5
25.0
22.5
(Feb) Mar-Jul
Jul-Dec
EW1 EW2 EW3 EW4 EW5 LW1 LW2 LW3 LW4 LW5
Tree-ring section
(e)
Precipitation δ18O (‰)
5
0
-5
-10
-15
Jan Feb Mar Apr May Jun Jul Aug Sep Oct Nov Dec
Month

927

Figure 2 (a) Schematic figure for the intra-annual tree-ring section assignment following the tracheidogram method. The letter n and m represent the number of the EW and LW sections in a ring. In the example, a ring was split into 6 EW sections and 7 LW sections. Variability of $\delta^{18}O$ in each tree-ring section for (b) EW and (c) LW based on the method in panel a. (d) Mean values of tree-ring $\delta^{18}O$ for subsequent sections follow a "V" pattern. Horizontal bars at the bottom of the panel (d) represent the growing season length based on micro-coring measurements inferred from another study (Huang et al., 2018): light grey for EW and dark grey for LW. (e) Intra-annual pattern of precipitation $\delta^{18}O$ from ISOGSM model output and validated by the observational precipitation $\delta^{18}O$ at the Changsha station (Fig S3). Shaded area in panel (e) corresponds to the growing season in our study area.

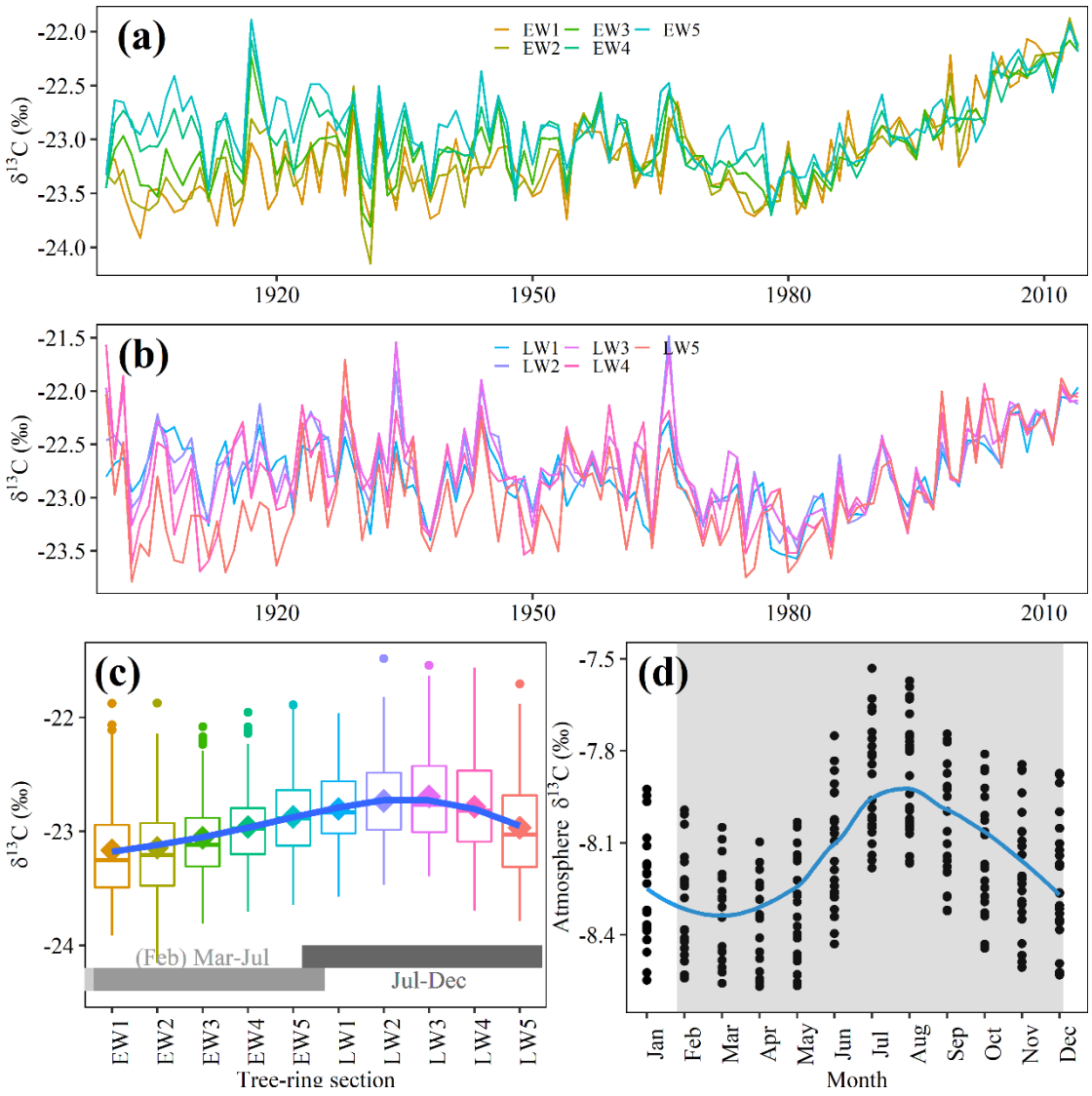

939

940 **Figure 3** Variability of $\delta^{13}C_{cor}$ in each tree-ring section for (a) Early-wood (EW) and
941 (b) late-wood (LW) based on the method in Figure 2a. (c) Mean values of tree-ring
942 $\delta^{13}C_{cor}$ for subsequent sections follow an asymmetric inverse-V pattern. Bars at the
943 bottom of panel c represent the growing season length based on micro-coring
944 measurements inferred from another study (Huang et al., 2018): light grey for EW and
945 dark grey for LW. (d) The intra-annual pattern of atmospheric $\delta^{13}C$ ($\delta^{13}C_{atm}$) at the
946 Waliguan station from 1990 to 2014. Shaded area in panel (d) corresponds to the
947 growing season in our study area.

948

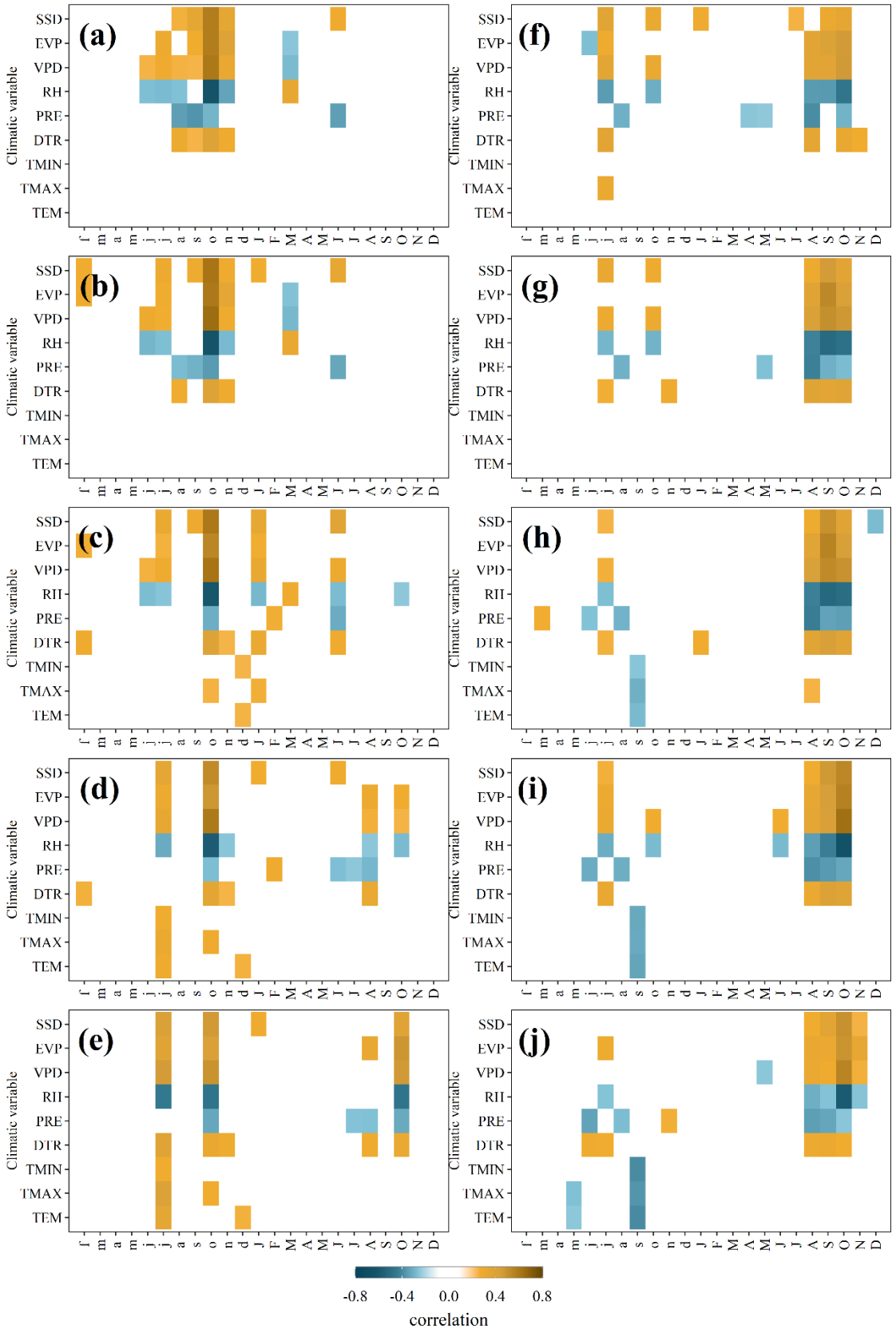
(a)
(b)
(c)
(d)
(e)
(f)
(g)
(h)
(i)
(j)
Climatic variable
SSD
EVP
VPD
RH
PRE
DTR
TMIN
TMAX
TEM
-0.8
-0.4
0.0
0.4
0.8
correlation

949

Figure 4 Climate response of tree-ring $\delta^{18}O$ for each EW and LW section. (a)-(e) correspond to EW sections EW1 to EW5, and (f)-(i) correspond to LW sections LW1 to LW5. Only significant Pearson's correlation coefficients ($p < 0.05$) are shown. On the X-axis, lowercase (uppercase) letters indicate the month of the previous (current) year. The climate variables include mean (TEM), maximum (TMAX), and minimum (TMIN) temperature, monthly diurnal temperature range (DTR), monthly precipitation (PRE), monthly relative humidity (RH), monthly vapor pressure deficit (VPD), monthly diurnal evaporation (EVP), and monthly sunshine duration hours (SSD).

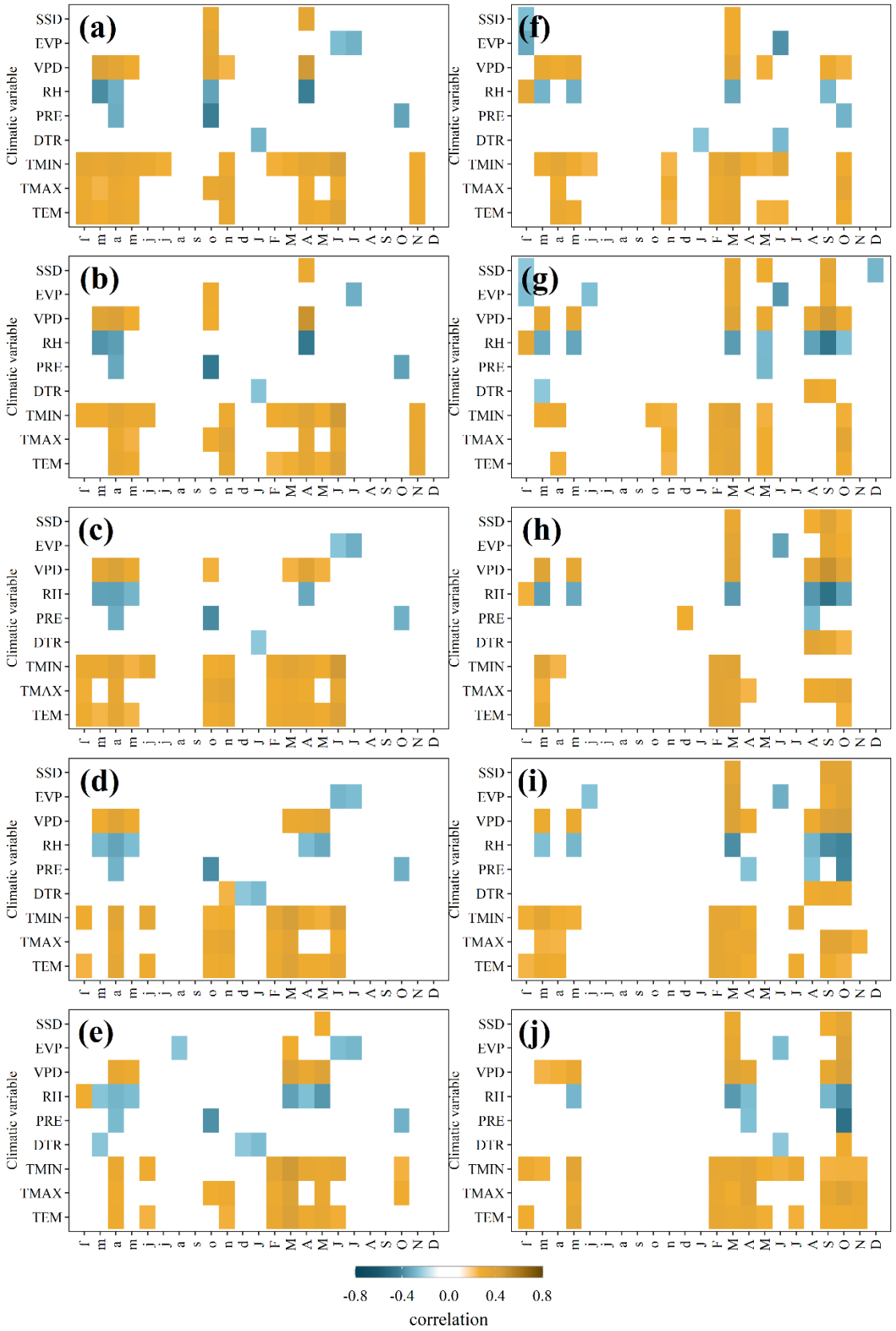

958

959 **Figure 5** Same as Figure 4 but for tree-ring $\delta^{13}C_{cor}$.

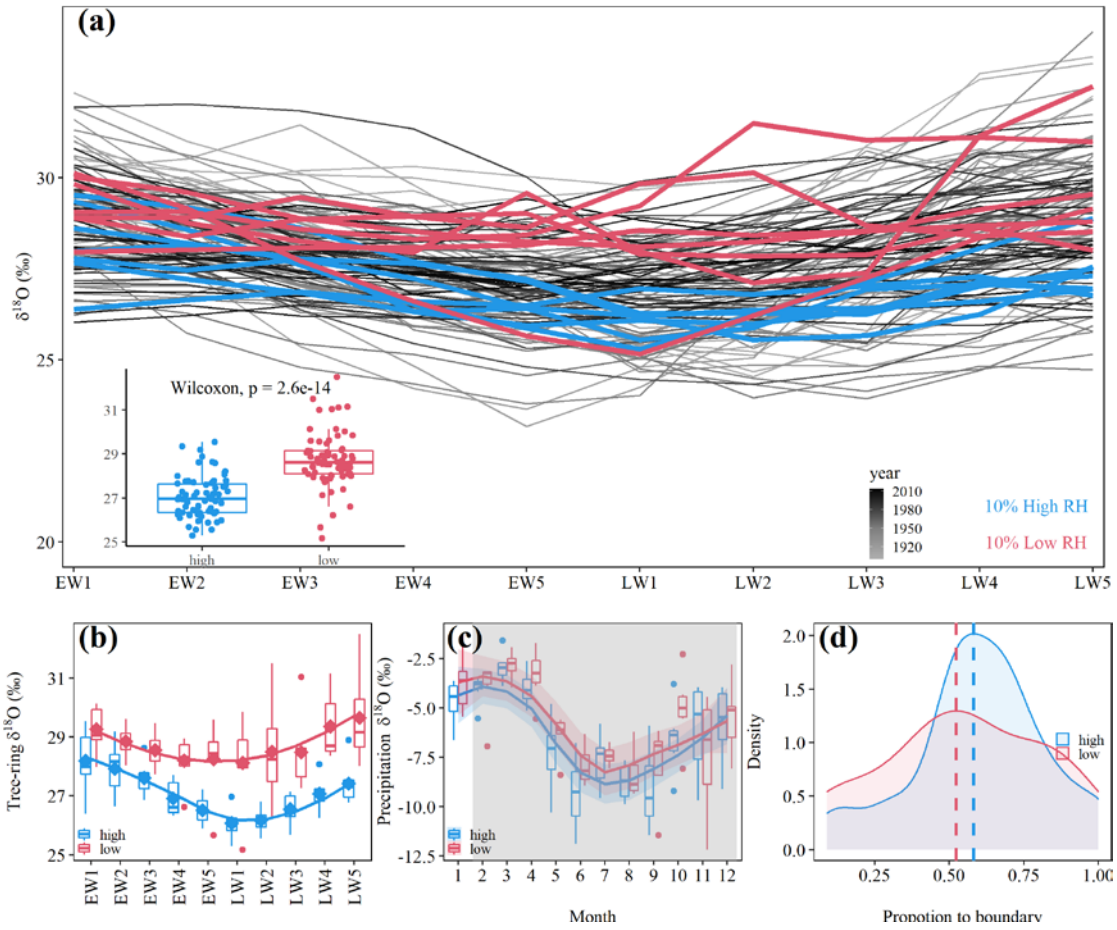

960

961 **Figure 6** Intra-annual profile of tree-ring $\delta^{18}O$ for each year (a). The insert figure in
962 panel a is the comparison of the mean $\delta^{18}O$ values for dry (red) and wet (blue) years,
963 which are determined by the 10th and 90th percentile, respectively, of the growing
964 season relative humidity during the period 1953-2014. Intra-annual mean tree-ring $\delta^{18}O$
965 (b) and monthly precipitation $\delta^{18}O$ (c) in dry versus wet years. Density diagram of the
966 position of minimum tree-ring $\delta^{18}O$ in dry versus wet years (d) and vertical lines
967 represent maximum density.

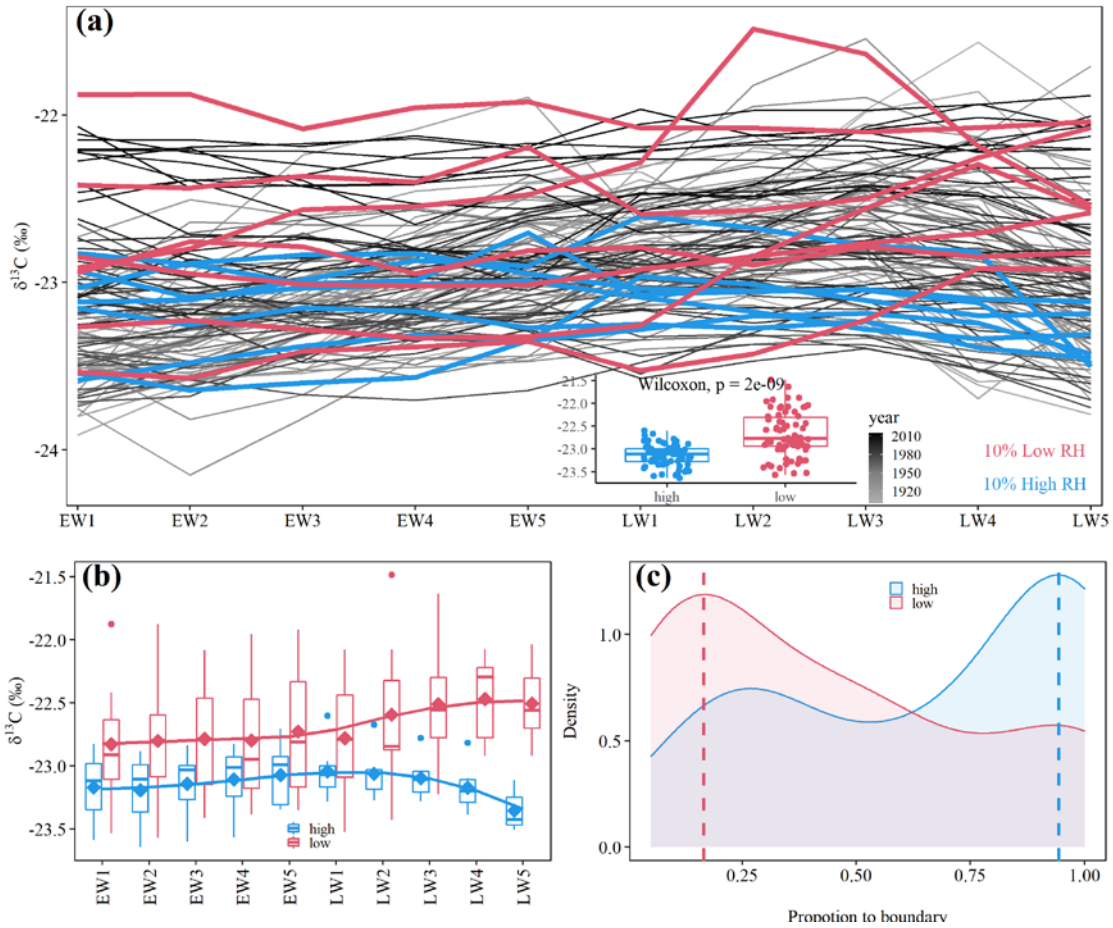

968

969 **Figure 7** Same as Figure 6 (a) and (b) but for tree-ring $\delta^{13}C_{cor}$. Density diagram of the

970 position of minimum tree-ring $\delta^{13}C_{cor}$ in atmospheric dry and wet years (c) and vertical

971 lines represent maximum density.

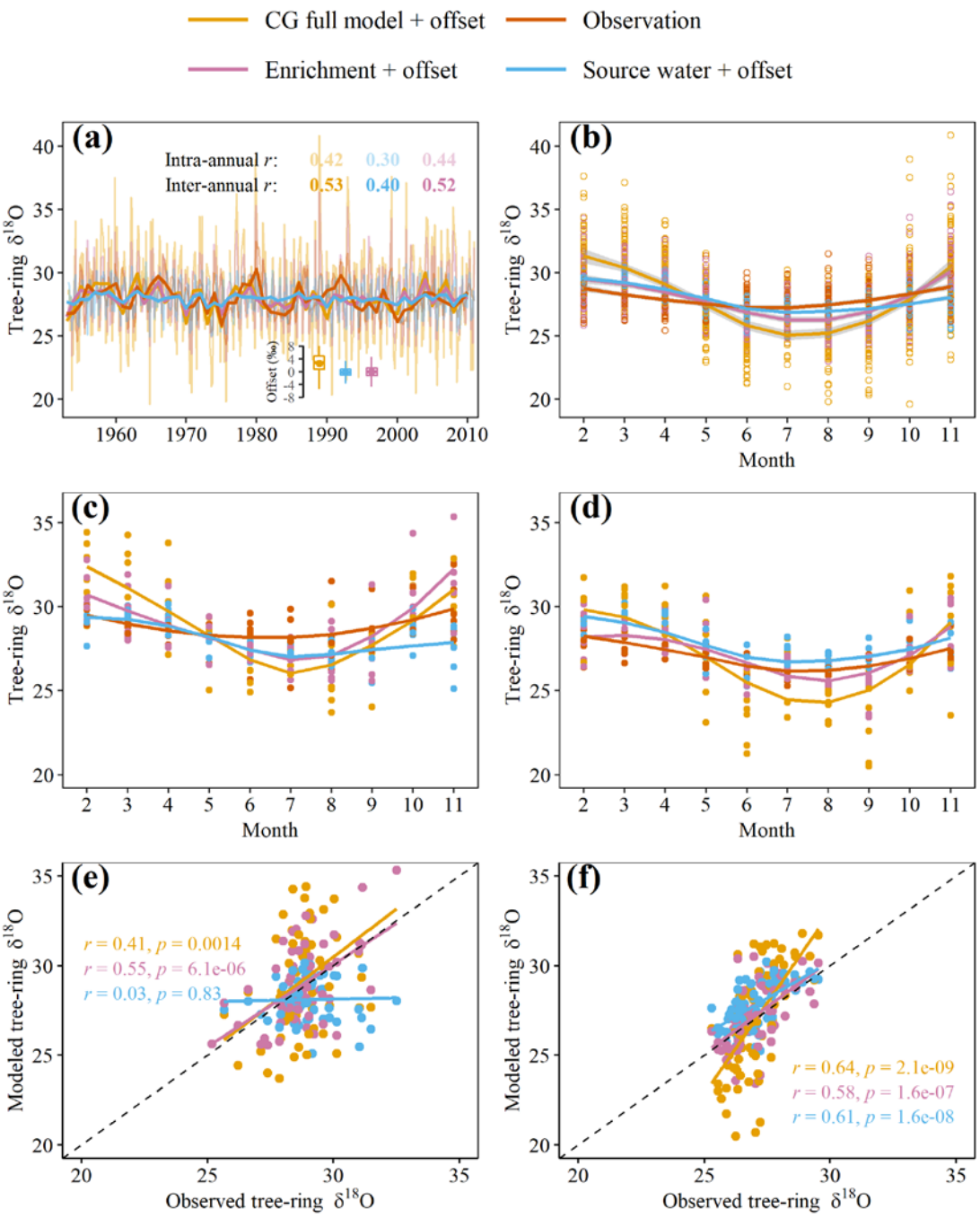

Figure 8 Comparison between modeled and measured tree-ring $\delta^{18}O$. (a) interannual variability (intra-annual scale: lighter color, year-to-year: dark color) and (b) intra-annual profiles. The inserted boxplot in panel (a) shows the offset (whiskers for the 1.5 interquartile range, and the dot for the mean) between observations and model simulations. Significant Pearson correlations (p < 0.01) between observation and simulation are shown in panel (a). The details of the model (such as full name and inputs)

can be found in Table 1 and S2 and we defined February-November as the growing season in all model runs. Comparisons of the intra-annual profiles of tree-ring $\delta^{18}O$ between measured and modeled $\delta^{18}O$ during (c) dry years and (d) wet years. Scatter plot of measured and modeled tree-ring $\delta^{18}O$ during (e) dry and (f) wet years. Pearson correlation coefficients between observations and model simulations and significance level are shown. Diagonal dashed lines in (e) and (f) are 1:1 lines.

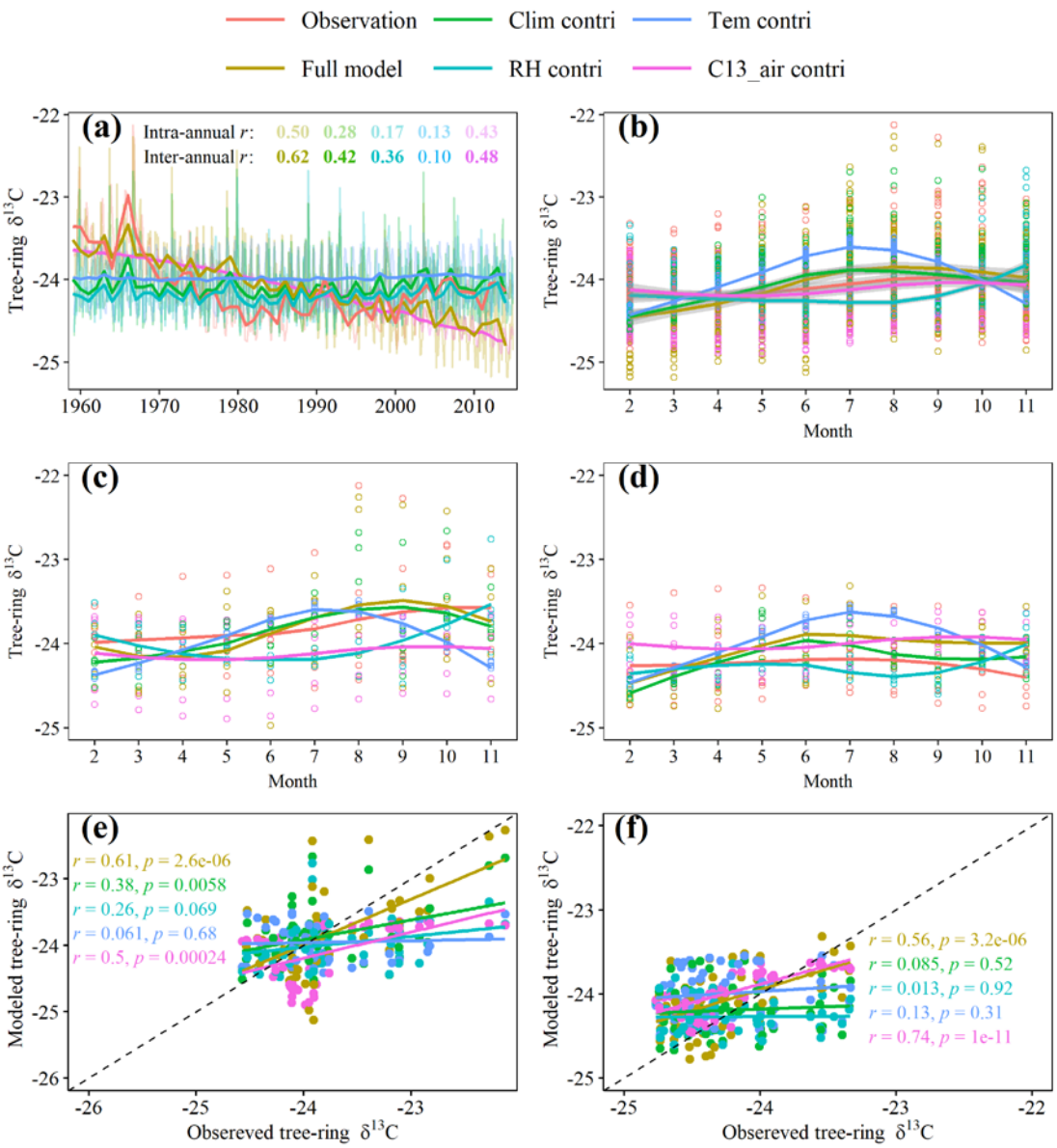

985

986 **Figure 9** Comparison between modeled and measured tree-ring $\delta^{13}C$ for (a) interannual
987 variability (intra-annual: lighter color, year-to-year: dark color) and (b) intra-annual
988 profiles. Pearson correlation coefficients between observations and simulations are
989 shown in panel a (bold type, $p < 0.01$; and regular type, insignificant). The modeling
990 procedure consisted of varying one contributing parameter at a time with the other
991 parameters remaining constant (the mean value for 1953-2010). The full model
992 included all varying parameters. The details of the model (such as full name and inputs)
993 can be found in Table 1 and S2 and we defined February-November as the growing
994 season in all model runs. Comparison of the intra-annual profiles of measured and

modeled $\delta^{13}C$ during (c) dry years and (d) wet years. Scatter plot of measured and modeled tree-ring $\delta^{13}C$ during (e) dry and (f) wet years. The Pearson correlation coefficients between observations and model simulations and significance levels are shown. Diagonal dashed lines in (e) and (f) are 1:1 lines.

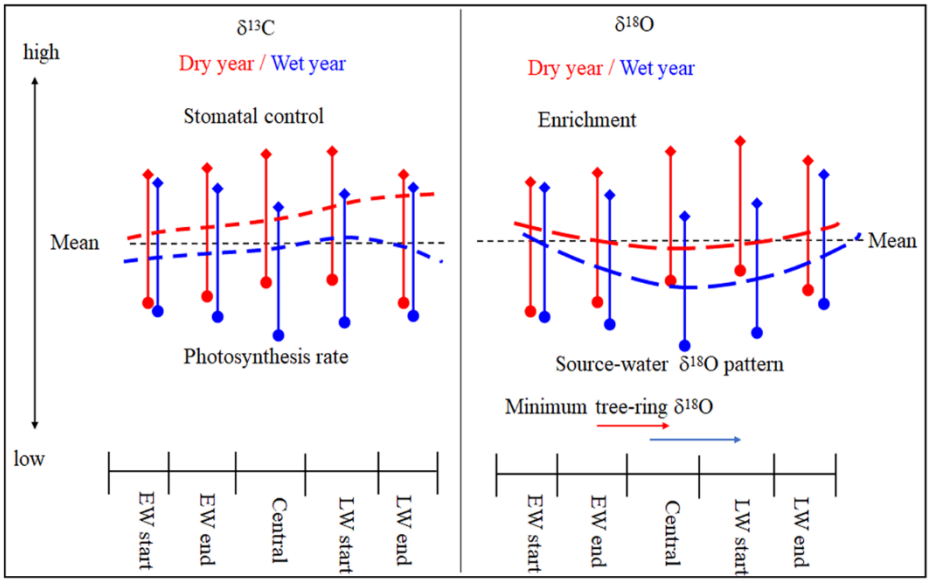

Figure 10 Schematic diagram of a potential main controlling process of intra-annual tree-ring $\delta^{18}O$ and $\delta^{13}C$ profiles in wet and dry years. Left panel is for $\delta^{13}C$ and right is for $\delta^{18}O$.Diamonds and dots indicate the positive and negative effects, respectively. The colored dashed lines indicate intra-annual profiles of tree-ring $\delta^{13}C$ and $\delta^{18}O$ in wet years (blue) and dry years (red). The length of the vertical line above or below the mean indicates the relative contributions of the main controlling processes: stomatal control and photosynthesis rate for $\delta^{13}C$ and leaf-water enrichment and source-water $\delta^{18}O$ for tree-ring $\delta^{18}O$. The X-axis represents the different sections of tree rings. The horizontal arrows in the right panel indicate the probability of position of tree-ring $\delta^{18}O$ minima in wet (blue) and dry (red) years.